communications earth & environment

ARTICLE

https://doi.org/10.1038/s43247-021-00130-w OPEN

Past megadroughts in central Europe were longer, more severe and less warm than modern droughts

M. Ionita [1✉], M. Dima[1,2], V. Nagavciuc[1,3], P. Scholz[1] & G. Lohmann [1,4]

Megadroughts are notable manifestations of the American Southwest, but not so much of the European climate. By using long-term hydrological and meteorological observations, as well as paleoclimate reconstructions, here we show that central Europe has experienced much longer and severe droughts during the Spörer Minimum (~AD 1400–1480) and Dalton Minimum (~AD 1770–1840), than the ones observed during the 21st century. These two megadroughts appear to be linked with a cold state of the North Atlantic Ocean and enhanced winter atmospheric blocking activity over the British Isles and western part of Europe, concurrent with reduced solar forcing and explosive volcanism. Moreover, we show that the recent drought events (e.g., 2003, 2015, and 2018), are within the range of natural variability and they are not unprecedented over the last millennium.

[1] Alfred Wegner Institute Helmholtz Center for Polar and Marine Research, Bremerhaven, Germany. [2] Faculty of Physics, Bucharest University, Bucharest, Romania. [3] Faculty of Forestry, Ștefan cel Mare University, Suceava, Romania. [4] MARUM, Bremen University, Bremen, Germany. ✉email: Monica.Ionita@awi.de

Drought is one of the most expensive and damaging natural disasters, which commonly affects large areas and can last for several months to years. Since the beginning of the 21st century, Europe has experienced a series of long-lasting dry and hot summers (2003, 2010, 2013, 2015, and 2018)[1–5]. This type of hydroclimatic extreme can affect all components of the hydrological cycle and it is, usually, associated with significant socio-economic losses[6]. If the deficit in precipitation is combined with high evapotranspiration losses, then it can lead to a deficit in soil moisture and subsequently can manifest itself as a hydrological drought, i.e., deficits in streamflow and groundwater[7]. Prolonged major droughts with severe impacts, such as those recorded in 2003 and 2015 have highlighted Europe's vulnerability to this natural hazard and alerted governments, stakeholders, and operational agencies about the disastrous effects droughts may have on the society and economy, including the need for mitigation measures[8–10]. In 2018, the central part of Europe, especially Germany, experienced the warmest April-to-July months since 1880 (Supplementary Fig. 1a) and in some locations all-time maximum temperatures were recorded. This situation was exacerbated by a rainfall deficit from February to November 2018 (Supplementary Fig. 1b), when the average precipitation reached, on average, just 58% of the climatological rainfall amount. The analysis shows that this particular long-lasting warm and dry year was produced and maintained by a long-lived blocking event[5,11].

Although the scientific community has attributed the occurrence of these extreme events to anthropogenic climate change[11–13], the instrumental record of precipitation, temperature, and soil moisture is sparse and the satellite record too short, making it difficult to assess whether the 21st-century drying is without precedent. Multicentennial reconstructions of past temperatures for the central part of Europe indicate that the recent summer warming is unprecedented over the last 2500 years[14,15]. Coincident with this increase in temperature, different regions of the European continent have experienced prolonged and severe droughts since the early 2000s[1,2,4,16], attributed, among other factors, to rising land and ocean temperatures[1,17,18]. For example, the extreme drought events at the European level, in 2003, 2015, and 2018, have been exacerbated by the elevated temperatures[1,12,19,20], which makes these events unusual during the instrumental period[11,12]. Although these events appear to be unprecedented in terms of temperature contribution, they were also unusual in terms of other characteristics (e.g., magnitude and/or duration). Thus, a comprehensive understanding of the causes and mechanisms of these unusual episodes requires investigations from a long-term perspective.

Here we construct a millennial view for these events, based on long-term hydrological and meteorological data as well as paleoclimate reconstructions of the Palmer Drought Severity Index (PDSI) extracted from the Old World Drought Atlas (OWDA)[21], for the central part of Europe. In this respect, we make use of a 1000-years tree ring reconstruction of summer drought at European level[21], to evaluate whether the recent drying was unprecedented in its joint duration and severity over the Common era. The focus here is on central Europe (black square in Fig. 1a), given that in 2015 and 2018 this was the most affected region by the extreme drying and that a rich database of climate reconstructions is available for an in-depth evaluation of the drought occurrence over the last millennium. We also make use of sea surface temperature (SST), sea surface salinity, and large-scale atmospheric circulation reconstructions and paleo reanalysis to investigate the driving mechanism behind the dry periods over the last millennium.

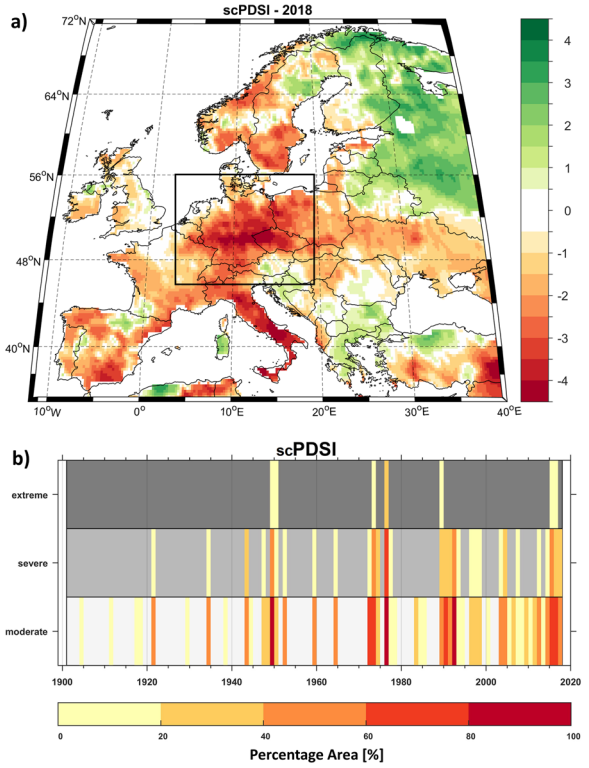

Fig. 1 Present-day drought variability. a Self-calibrated Palmer Drought Severity Index (scPDSI) for summer 2018[50] and (**b**) Temporal evolution of the percentage area of central Europe affected by droughts for three drought severity categories: moderate (white), severe (gray) and extreme (dark gray). Moderate drought is defined as $-3 < \text{scPDSI} \leq -2$; severe drought is defined as $-4 < \text{scPDSI} \leq -3$ and severe drought is defined as $\text{scPDSI} \leq -4$.

Results and discussion

The reconstructed PDSI index, based on the OWDA, for the analyzed region accounts for 52 % ($r = 0.71$, $p \ll 0.001$) of the variability in the observed self-calibrated Palmer Drought Severity Index (scPDSI index) over the common period (1901–2012) (Fig. 2a). For the common period (1901–2012), the driest years are 1921 and 1976, respectively (Figs. 1b and 2a). The years 1102, 1503, 1865, and 1921 are recorded as the driest ones over the last millennium, based on the OWDA data (Fig. 2a), while summers 1949, 1976, and 1990 are recorded as the driest ones over the observational period, based on the observed scPDSI (Fig. 1b). The 1921 drought had a higher amplitude over the north-western part of Germany (Supplementary Fig. 2), while the 1976 drought was recorded over the whole analyzed region. These aspects are also captured by the low-flow situation on the Rhine, Elbe, and Weser rivers (Supplementary Fig. 3). The year 1921 ranks also as the driest in the Rhine and Weser catchment areas (Supplementary Fig. 3b and 3c) (both situated in the western part of Germany). The years 2003, 2015, and 2018 do not rank among the top driest years either in the reconstructed PDSI or in the observed records. From 1810 onwards, the driest years (1865, 1893, 1921, 1947, 1976, and 2003), as captured by the reconstructed PDSI index, correspond also to extremely dry years, in terms of low flow periods, in the observed streamflow data for the most important rivers in central Europe (the Rhine, Elbe, and Weser, Supplementary Fig. 3). This is an indication that the reconstructed PDSI index can properly capture the occurrence of drought events over the analyzed period, and can be used to place the 21st-century droughts into a long-term context. From the perspective of the

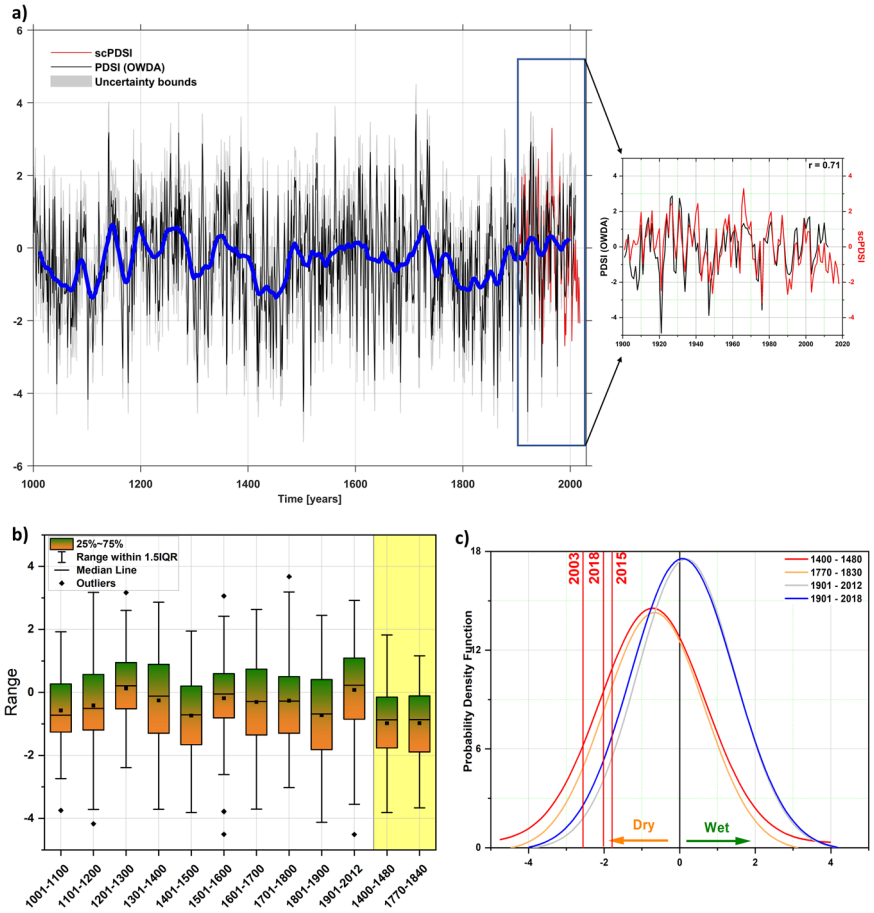

Fig. 2 Drought events from a long-term perspective. a Regional mean Old World Drought Atlas (OWDA)[21] PDSI index for central Europe (3°E-20°E, 45° N-56°N, black line) for the 1000–2012 period and the instrumental[50] June through August scPDSI (solid red line) for the 1901–2018 period. Uncertainty (1σ) calculated as the root-mean-squared error from the residual fit to the instrumental series shown as the shaded gray region. The blue line represents the 31 years running mean of the OWDA time series; (**b**) Comparison between the reconstructed PDSI index (black line)[21] and the observed scPDSI index (red line)[50] over the common period: 1901–2012; (**c**) The fitted Gaussian distribution of the reconstructed PDSI[21] values for different time periods: 1400–1480 (red line), 1770–1840 (orange line), 1901–2012 (gray line) and for the observational data[50] for the period 1901–2018 (blue line). The values for 2003, 2015, and 2018 are indicated with a red line. The OWDA record has been adjusted by the mean and standard deviation so that it has the same mean and standard deviation as the instrumental data.

last ~1000 years, the 20th century and the beginning of the 21st century are characterized by reduced multidecadal variability in the occurrence of dry and wet periods, mainly when compared with the previous centuries (Fig. 2a). The driest years, over the last millennium, in the central part of Europe are 1102, 1419, 1503, 1504, 1858, 1865, and 1921, respectively (Fig. 2a and Supplementary Fig. 4).

Two megadroughts in central Europe. Throughout the last millennium, two distinct and long-lasting dry periods, so-called megadroughts, are observed: one over the ~1400–1480 period, and the other over the ~1770–1840's time interval (Fig. 2a, b). The mid-15th century megadrought largely was synchronous with the Spörer Minimum (1420–1550), a period of low solar activity with the strongest reduction in incoming total solar irradiance (TSI)[22], which was punctuated also with several large volcanic eruptions[23]. In Western Europe, the early Spörer Minimum was coincident with a series of extremely cold and long-lasting winters[24–27], which had a dramatic effect on the productivity of terrestrial ecosystems in the subsequent growing seasons, manifested also as devastating losses in agricultural production. Based on documentary evidence[28], here we show that the 1400–1480 megadrought event was characterized by dry summers (the driest decade over the last millennium was recorded between 1471 and 1480, Fig. 3d), and colder than average winters (Fig. 4b) and springs (Fig. 4c). A tree-ring based reconstruction of spring (AMJ) precipitation (Supplementary Fig. 5d) and summer (JJA) temperature (Supplementary Fig. 5e), over a larger region covering the western and central parts of Europe, indicates that this period was characterized by a decline in the mid-spring precipitation and cold summers, especially over the 1440–1480[29] period.

Similarly, the 1800's megadrought corresponds to the Dalton Minimum (1790–1830), also a period of low solar activity and several volcanic eruptions, which coincided with a period of lower-than-average global temperatures. During this period, there was a variation in temperature of about −1 °C in the central part of Europe[28,30]. The 1770–1840's megadrought event is associated with one of the driest periods over the last millennium (Fig. 3). Winter, spring, and summer seasons were all characterized by negative precipitation anomalies over more than five consecutive decades (Fig. 3b–d) and colder than normal winters and springs (Fig. 4c, c). This extremely dry period was accompanied by cold and harsh long-lasting winters in the Baltic Sea[31]. The second megadrought event (~1770–1840) is clearly captured also by a new reconstruction of the Standardized Precipitation Index over

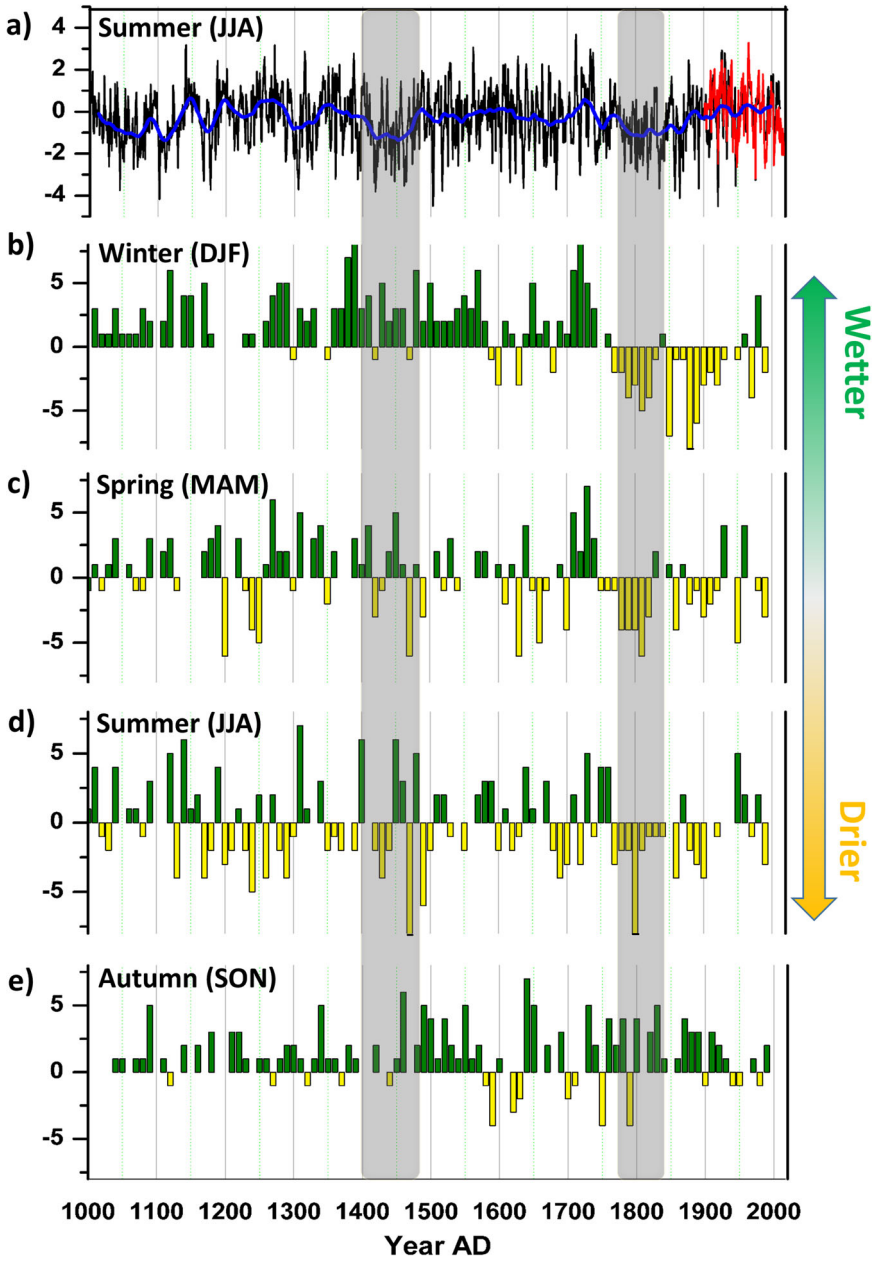

Fig. 3 Precipitation variability over the last millennium. a Regional mean Old World Drought Atlas (OWDA)[21] PDSI index for central Europe (3°E-20°E, 45°N-56°N, black line) for the 1000–2012 period and the instrumental June through August scPDSI[50] (solid red line) for the 1901–2018 period; Decadal frequency of the seasonal precipitation over the central part of Europe based on proxy reconstructions and documentary evidence: (**b**) winter; (**c**) spring; (**d**) summer and (**e**) autumn. The seasonal precipitation data is based on the seasonal decadal precipitation index from Glaser (2013)[28].

Germany, for the last 500 years (Supplementary Fig. 5b)[32]. This event was also observed in Poland, where the 1770–1840 period was characterized by long-lasting dry events and precipitation deficit (Supplementary Fig. 5c). In other reconstructions[29,33,34], spanning the last millennium, the driest period was recorded between 1770 and 1820 (Supplementary Figs. 5, 6, and 7), while over the 1820–1840 period altering of dry/wet years can be observed. The differences between the different data sets employed at the end of the second megadrought (~1820–1840), might be due to the different types of proxy data used to derive the reconstructions and their uncertainties.

To emphasize the differences between the two megadroughts and the present-day drought variability, in Fig. 2c we show the statistical distribution of reconstructed PDSI (OWDA) index for three distinct periods, corresponding to the two megadrought events (1400–1480—red line; 1770–1840—orange line, and the 1901–2012 period gray line), and of the observed scPDSI index over the 1901–2018 period (blue line). The Gaussian distribution fitted over the four periods shows that there is a significant difference in the distribution of the two mega-dry periods when compared to the 20th and 21st century drought events, indicating that the megadroughts are associated with anomalous climate regimes. From Fig. 2c we can infer that the 2003, 2015, and 2018 droughts are not unprecedented over the last millennium.

Links between solar forcing and the megadroughts. Numerical integrations indicate that high/low solar irradiance levels are generating weak/strong AMOC states, a few decades later[35,36]. Consistent with this, the TSI maxima just before 1400, 1600, and

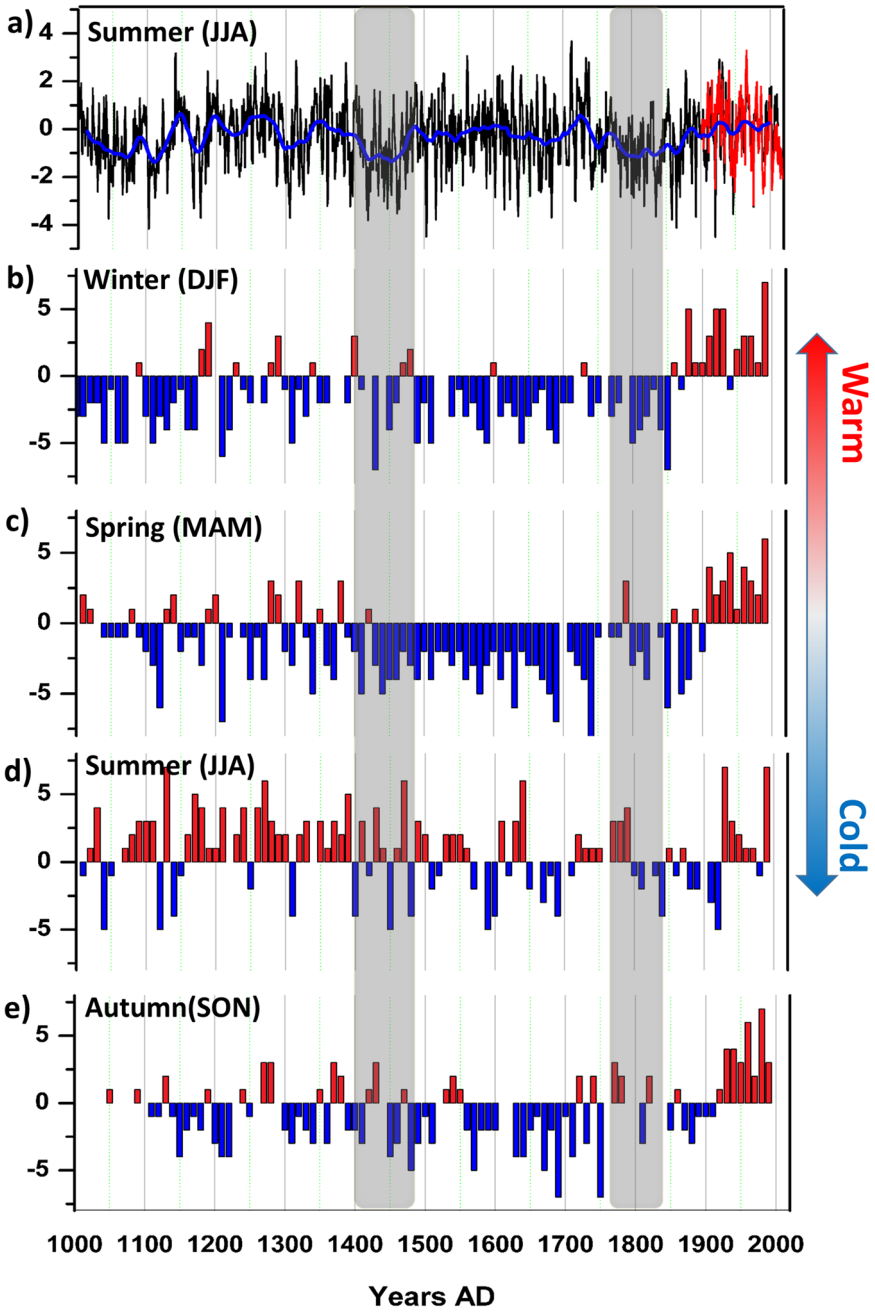

Fig. 4 Temperature variability over the last millennium. a Regional mean Old World Drought Atlas (OWDA)[21] PDSI index for central Europe (3°E-20°E, 45°N-56°N, black line) for the 1000–2012 period and the instrumental June through August scPDSI[50] (solid red line) for the 1901–2018 period; Decadal frequency of the seasonal temperature over the central part of Europe based on proxy reconstructions and documentary evidence: (**b**) winter; (**c**) spring; (**d**) summer and (**e**) autumn. The seasonal temperature data is based on the seasonal decadal temperature index from Glaser (2013)[28].

1800 are followed by weak Atlantic Meridional Overturning Circulation (AMOC) episodes, a few decades later (Fig. 5d)[37]. Due to the fact that TSI evolves from a positive to a negative also in several decades, the weak AMOC state is quasi-synchronous with the TSI minima (Fig. 5d–f). Model simulations show also that a negative Atlantic Multidecadal Oscillation (AMO)/ weak AMOC state induces an in-phase baroclinic atmospheric response consisting of a high-pressure system extending from eastern North Atlantic towards northern and central Europe[38,39]. A similar atmospheric structure, e.g., an anticyclonic circulation over the British Isles and the western part of Europe, associated with periods of low solar activity, is derived based on proxy and paleo reanalysis data (Fig. 6a, b). Therefore, through this causal chain, TSI minima are associated with such a high-pressure system, consistent with numerical integrations[40,41]. The atmospheric center of positive Z500 anomalies (Fig. 6) largely suppresses ascending motions, reduces water vapor condensation and precipitation formation, leading to drought conditions below this atmospheric system. This effect is amplified by the inherent persistence of this typical blocking configuration. Consistent with this, dry summers are associated with a seasonally persistent high-pressure system (from winter to summer) centered over the British Isles and the western part of Europe (Supplementary Fig. 8). The association between cold North Atlantic conditions, the high-pressure system and the dry summers in central and northern parts of Europe manifests also over the observational

period, when extended dry periods over the analyzed region (e.g., 1971–1976) (Fig. 7a) occurred in combination with a cold North Atlantic basin (Fig. 7c) and enhanced atmospheric blocking over the central part of Europe (Fig. 7d). The 1971–1976 time interval was characterized also by an abrupt AMOC weakening[42].

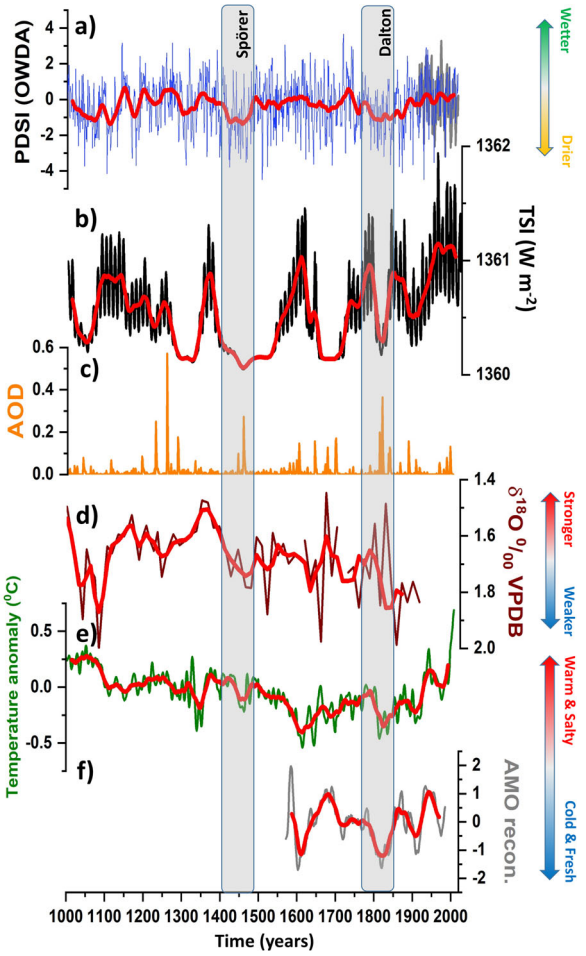

Fig. 5 Climate variability over the last millennium. a Regional mean Old World Drought Atlas (OWDA) PDSI index[21] for central Europe (3°E-20°E, 45°N-56°N, black line) for the 1000–2012 period and the instrumental[50] June through August scPDSI (solid red line) for the 1901–2018 period; (**b**) Time series of annual total solar irradiance[63]; (**c**) Aerosol optical depth (AOD)[64]; (**d**) $\delta^{18}O$ (*T. quinqueloba*) measurements of planktonic foraminifera as a proxy for changes in the surface hydrography of the eastern Labrador Sea over the last millenium[65]; (**e**) Reconstructed Atlantic Multidecadal Oscillation index (AMO)[66] and (**f**) as in (**e**) but based on tree rings[48].

The two megadroughts over the central part of Europe and their relationship with the prevailing SSTs in the North Atlantic basin are visible also in two paleo reanalyzes of the last millennium (Supplementary Figs. 7, 9, and 10)[33,34], although the amplitude of the megadroughts in the paleo reanalysis data is smaller compared to the amplitude of these two events in the Old World Drought Atlas (OWDA) reconstruction (Supplementary Fig. 7). These links between cold North Atlantic conditions and European scale drought are supported also by previous studies based on observational data[42–44]. Similarly, it was shown that during the negative phase of AMO (cold North Atlantic basin) Germany and the southern part of the Scandinavian Peninsula is affected by dryness, while a warm North Atlantic basin (positive AMO phase) is associated with wetness over these regions[45]. The canonical understanding of oceanic influences on European droughts suggests that, on multidecadal time scales, summer drought variability over the central and western part of Europe is strongly associated with the variability of the North Atlantic SSTs in the previous winter[42]. In general, dry (wet) summers over the central and western parts of Europe are associated with cold (warm) SSTs in the North Atlantic basin in the previous winter (Fig. 7 and Supplementary Fig. 11).

Here we used independent reanalysis data sets and proxy records to show that, concurrent with low solar activity, cold North Atlantic conditions linked to weak AMOC states are associated with a high-pressure system located over central and northwestern Europe and enhanced blocking activity (Fig. 7), resulting in long-lasting dry periods in the mid-15th century and the beginning of the 18th century. Unlike the megadroughts throughout the last millennium, the worst-case droughts of the 21st century (e.g., 2003, 2015, or 2018) are also amplified by the extremely warm summers, in association with the global warming, which will likely exacerbate drought over the European continent[46]. The fact that for other solar minima periods (e.g., Maunder Minimum, ~1655–1715) we do not see dry periods over the western part of Europe, indicates that the 15th and 18th-century megadroughts are the response to both internal and forced climate variability. During the Maunder Minimum, paleoclimate reconstructions indicate that the North Atlantic was warmer compared to the Spörer and Dalton minimum time intervals (Fig. 5)[47] and that AMO was in a positive phase[48]. This period was associated with precipitation excedent over our analyzed region (Fig. 3). Thus, the two western European megadroughts might have been the result of an interplay between solar extremes, cold North Atlantic surface waters, enhanced blocking activity and explosive volcanism.

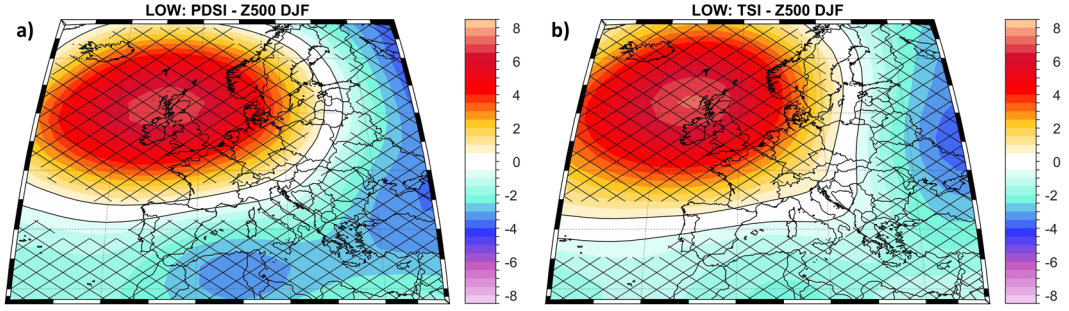

Fig. 6 Large-scale climate drivers of dry events. a The low composite map between the reconstructed[21] PDSI index (PDSI < − 0.75 std. dev.) and winter reconstructed Geopotential Height at 500 mb (Z500)[53] and (**b**) the low composite map between the reconstructed TSI[63] (TSI <−0.75 std. dev.) and winter reconstructed Geopotential Height at 500 mb (Z500)[53]. The hatching highlights significant values at a confidence level of 95 %. Analyzed period: 1500–1999. Units: Z500 (m).

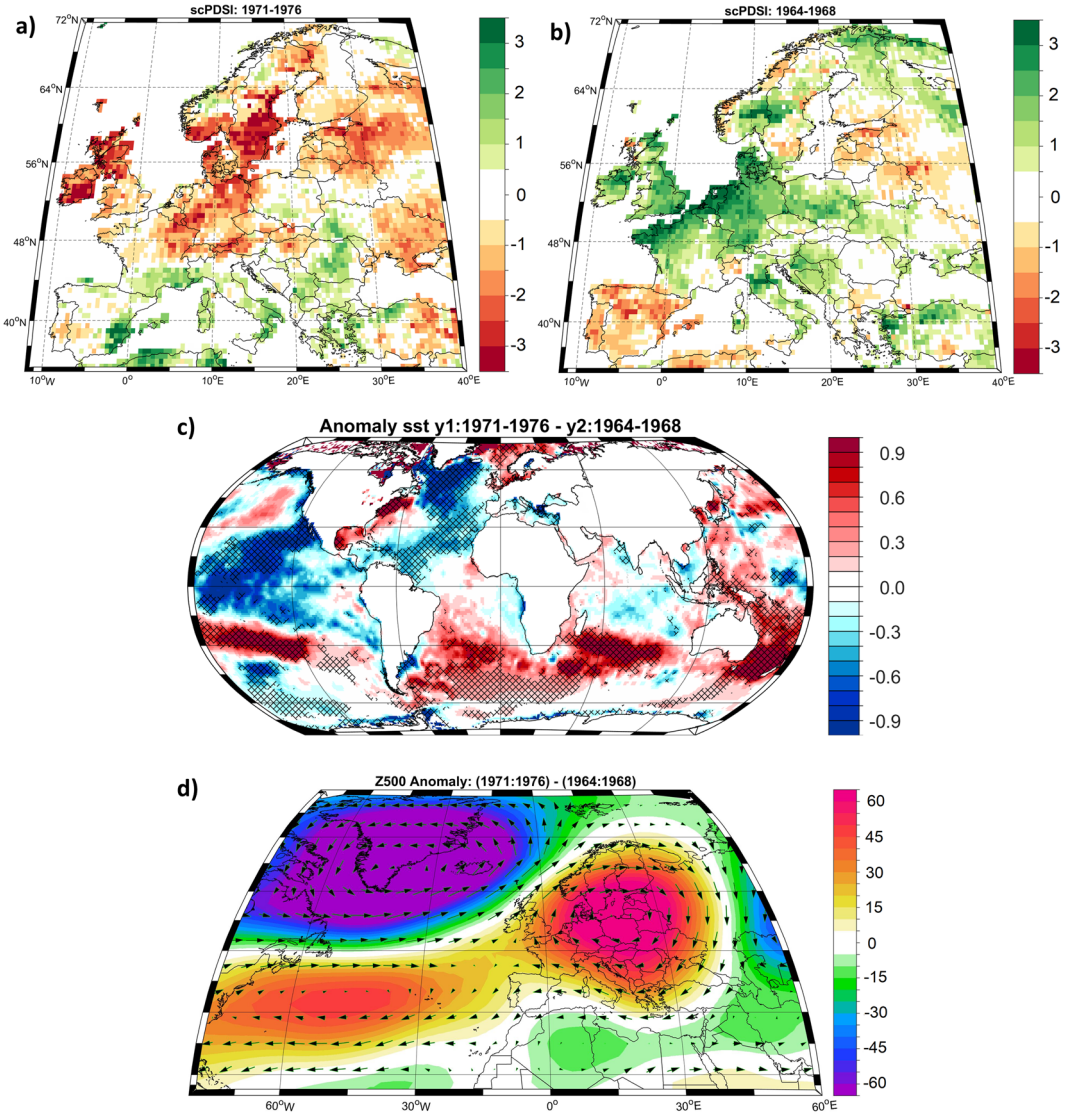

Fig. 7 Large-scale atmospheric and oceanic drivers of dry periods. a Observed[50] summer scPDSI averaged over the 1971–1976 period; (**b**) as in (**a**) but for the 1964–1968 period; (**c**) The winter SST anomaly[51] computed as the difference between the period (1971–1976) and (1964–1968); as in **c**) but for the winter gepotential height and wind (vectors) at 500 mb level (Z500)[52]. The hatching in (**c**) highlights significant values at a confidence level of 95%. Units: (**c**) SST (°C) and (**d**) Z500 (m).

Conclusions

By using different independent data sets (e.g., observations, paleo reanalysis, documentary evidence, and proxy records) in this study we provide a comprehensive assessment of past mega-droughts in central Europe and their underlying drivers. Moreover, we have shown that the recent droughts (e.g., 2003, 2015, and 2018, among others) are within the historical variability and they are not unprecedented over the last millennium. Future climate projections indicate that Europe will face substantial drying, even for the least aggressive pathways scenarios (SSP126 and SSP245)[49]. Although the greenhouse gases and the associate global warming signal will substantially contribute to future drought risk[49], our study indicates that future drought variations will also be strongly influenced by natural variations. A potential decrease of TSI in the next decades could result in a higher frequency of drought events in central Europe, which could add to the drying induced by anthropogenic forcing. The potential manifestation of record extreme droughts represents a possible scenario for the future and it would represent an enormous challenge for the governments and society. Thus, determining future drought risk of the European droughts requires further work on how the combined effect of natural and anthropogenic factors will shape the drought magnitude and frequency.

Methods

Observational, reanalysis and proxy data. Observed precipitation, temperature, and scPDSI were obtained or calculated from the Climate Research Unit's TS 4.03 data product[50]. These fields have a 0.5° × 0.5° resolution. The streamflow data was provided by the German Hydrological Institute (www.bfg.de). As observed SST fields, we have used the HadISST data set, with a 1° × 1° resolution[51]. For the large-scale atmospheric circulation, we have used geopotential height, zonal and meridional wind at 500 mb from the 20th Century Reanalysis data[52], as well as reconstructed geopotential height at 500 mb (Z500) over the Eastern North Atlantic and Europe, back to 1500[53]. The seasonal reconstructed precipitation (Supplementary Fig. 6), over the European region, is based on two distinct data sources[54,55].

Drought reconstruction. From the Old World Drought Atlas (OWDA)[21] we extracted all grid points in the range 3°E–20°E and 45°N–56°N, for the 1000–2012 period and calculated a PDSI index, by averaging all the grid points from the

aforementioned region. To make valid seasonal comparisons to the current drought conditions based on observational records (CRU TS4)[50], we scaled the OWDA time series by the mean of the observations and verified their standard deviations. These two-time series are highly similar ($r = 0.71$, $p \ll 0.001$ for the 1901–2012 period and $r = 0.79$, $p \ll 0.001$ over the 1901–1978 period). We estimated the uncertainty in the scaled reconstruction by calculating the root-mean-squared error from the residual of the fit between the instrumental and original paleoclimate data. The results are shown in Fig. 1. One of the reasons for which we chose the current regional setup (e.g., central part of Europe) is also due to the fact that the OWDA has the proven capacity to reconstruct drought variability at multi-decadal time scales, especially over this region. The highest tree ring network, used in the OWDA development is located over Germany (Fig. S1 in Cook et al., 2015[21] paper). The OWDA shows the strong agreement with the seasonal precipitation reconstruction over Europe, for the last 500 years[55], especially in parts of central Europe (e.g., Germany, also in the pre-instrumental period).

Historical data. The data in Figs. 3 and 4 originate from different sources that cover the German territory and the neighboring countries (see Fig. 1 in Glaser and Riemann (2009)[56]). The seasonal decennial index represents the difference for each decade between too warm and too cold, and too wet and too dry years. The criterion for exceeding or falling below 'normal' events is the 0.75 standard deviation from the mean, relative to the period 1951–1980. A more detailed description of how the decennial index is computed is given in Glaser (2013)[28]. A wide range of historical data has been used to derive the seasonal decennial indices for temperature and precipitation, like annual town chronicles of German cities, family chronicles, diaries, newspapers, administrative records, harvest records, as well as proxy data (e.g., tree rings). Most of the data can be accessed at www.tambora.org, where a detailed description for each source type is given. To calibrate the precipitation and temperature indices extracted from the documentary data, instrumental data was used[28]. This index represents one of the longest and well-dated reconstruction in the central part of Europe regarding the seasonal variability of wet/dry and cold/warm regimes, over the last 1000 years.

Last millennium reanalysis. To test the potential linkages between the drought variability and the oceanic conditions over the last millennium, in this study we employ two last millennium reanalysis data: PHYDA data set[33] and Last Millennium Reanalysis (LMR) fields[34]. PHYDA reanalysis data is based on assimilation, a methodology that combines proxy information with global climate simulations[33]. PHYDA comprises information from a network of 2970 annually resolved proxies, together with the last millennium ensemble simulations based on the Community Earth System Model[57]. PHYDA outputs (e.g., PDSI and 2-m surface air temperature) span the years 0–2000 CE and have a spatial resolution of 2.5°lat × ~1.9°lon. This dataset has been developed with the specific aim of studying hydroclimate variability over the Common Era. PHYDA has been validated against observational data[33] and has been successfully employed to study oceanic and radiative forcing of the megadroughts in the American Southwest[58]. The Last Millennium Reanalysis (LMR)[34] uses an ensemble methodology to assimilate paleoclimate data to produce annually resolved climate field reconstructions of the Common Era (PDSI, SST, and geopotential height). LMR combines, through data assimilation, proxy data, and model climate simulations. The data assimilation is performed using a variant of the ensemble Kalman Filter. In this study, we use version 2.0[59], which includes the PAGES2K database[60,61] as a source for the proxy records and the CCSM4 last millennium simulations[62]. From the PAGES2K database, the only series which are annually resolved have been considered. LMR makes it possible to validate dynamical hypotheses for the causes of megadroughts throughout the simultaneous reconstruction of drought indices, ocean variables, and large-scale atmospheric circulation fields. Because the output of the LMR has an annual resolution, in this study we make use only of the global SST field, to study the relationship of the summer drought over the analyzed region in relationship with the global SST over the last millennium.

Composite analysis. To identify the physical mechanism responsible for the connection between the drought occurrence and the large-scale atmospheric circulation, we constructed the composite maps between the normalized time series of PDSI (TSI) for the years when the values of the index were lower than 0.75 std. dev (Fig. 6 and Supplementary Fig. 8). This threshold was chosen as a compromise between the strength of the climate anomalies associated with large-scale anomalies and the number of maps that satisfy this criterion. Further analysis has shown that the results are not sensitive to the exact threshold value used for our composite analysis (not shown). We have computed composite maps, instead of correlation maps, because the former reflect the nonlinearities included in the analyzed data. The significances of the composite maps are computed based on a standard t-test (confidence level 95%).

Data availability

No datasets were generated during this study. All data used in this study are publicly available from the sources cited in "Data and Methods".

Code availability

All code necessary to perform the reported analyses can be obtained from the corresponding author.

Received: 3 November 2020; Accepted: 17 February 2021;
Published online: 19 March 2021

References

1. Ionita, M. et al. The European 2015 drought from a climatological perspective. *Hydrol. Earth Syst. Sci.* **21**, 1397–1419 (2017).
2. Spinoni, J. et al. A new global database of meteorological drought events from 1951 to 2016. *J. Hydrol. Reg. Stud.* **22**, 100593 (2019).
3. Pfeiffer, M. & Ionita, M. Assessment of hydrologic alterations in Elbe and Rhine Rivers, Germany. *Water* **9**, 684 (2017).
4. Ionita, M., Nagavciuc, V., Kumar, R. & Rakovec, O. On the curious case of the recent decade, mid-spring precipitation deficit in central Europe. *npj Clim. Atmos. Sci* **3**, 49 (2020).
5. Bakke, S. J., Ionita, M. & Tallaksen, L. M. The 2018 northern European hydrological drought and its drivers in a historical perspective. *Hydrol. Earth Syst. Sci.* **24**, 5621–5653 (2020).
6. Stahl, K. et al. Impacts of European drought events: insights from an international database of text-based reports. *Nat. Hazards Earth Syst. Sci.* **16**, 801–819 (2016).
7. Tallaksen, L. M. & Van Lanen, H. A. J. Hydrological drought: processes and estimation methods for streamflow and groundwater. Dev. Water Sci. (2004).
8. Estrela, T., Menéndez, M., Dimas, M. & Marcuello, C. Sustainable water use in Europe. Part 3: extreme hydrological events: floods and droughts. *Environ. Issue Rep.* **21**, 1–84 (2001).
9. Kristensen, P., Iglesias, A., Sauri, D. & Agency, E. E. Water scarcity and droughts, Mapping the impacts of natural hazards and technological accidents in Europe, An overview of the last decade. EEA Technical Report (2010). https://doi.org/10.2800/62638
10. European Commssion. Communication from the Commission to the European Parliament, the Council, the European Economic and Social Committee and the Committee of the Regions: A Blueprint to Safeguard Europe's Water Resources. (2012).
11. Toreti, A. et al. The exceptional 2018 European Water Seesaw Calls for Action on Adaptation. *Earth's Futur* **7**, 652–663 (2019).
12. Schär, C. et al. The role of increasing temperature variability in European summer heatwaves. *Nature* **427**, 332–336 (2004).
13. Vogel, M. M., Zscheischler, J., Wartenburger, R., Dee, D. & Seneviratne, S. I. Concurrent 2018 Hot Extremes Across Northern Hemisphere Due to Human-Induced Climate Change. Earth's Fut. (2019). https://doi.org/10.1029/2019EF001189
14. Büntgen, U. et al. Tree-ring indicators of German summer drought over the last millennium. *Quat. Sci. Rev.* **29**, 1005–1016 (2010).
15. Neukom, R., Steiger, N., Gómez-Navarro, J. J., Wang, J. & Werner, J. P. No evidence for globally coherent warm and cold periods over the preindustrial Common Era. *Nature* **571**, 550–554 (2019).
16. Spinoni, J., Naumann, G., Vogt, J. V. & Barbosa, P. Meteorological droughts in Europe: events and impacts - past trends and future projections. (2016). https://doi.org/10.2788/79637
17. Spinoni, J., Naumann, G., Vogt, J. & Barbosa, P. European drought climatologies and trends based on a multi-indicator approach. *Glob. Planet. Change* **127**, 50–57 (2015).
18. Duchez, A. et al. Drivers of exceptionally cold North Atlantic Ocean temperatures and their link to the 2015 European heat wave. Environ. Res. Lett. 11, (2016).
19. Otto, F. 2015—a record breaking hot year. world weather attribution Available at: https://www.worldweatherattribution.org/record-hot-year-2015/.
20. Otto, F. Human contribution to the record-breaking July 2019 heatwave in France. world weather attribution (2019). Available at: https://www.worldweatherattribution.org/human-contribution-to-record-breaking-june-2019-heatwave-in-france/.
21. Cook, E. R. et al. Old World megadroughts and pluvials during the Common Era. Sci. Adv. (2015). https://doi.org/10.1126/sciadv.1500561
22. Eddy, J. A. Climate and the changing sun. Clim. Change (1977). https://doi.org/10.1007/BF01884410
23. Bauch, M. The day the sun turned blue: a volcanic eruption in the early 1460s and its possible climatic impact—a natural disaster perceived globally in the late middle ages? in 107–138 (2017). https://doi.org/10.1007/978-3-319-49163-9_6
24. Camenisch, C. et al. The 1430s: a cold period of extraordinary internal climate variability during the early Spörer Minimum with social and economic impacts in north-western and central Europe. *Clim. Past* **12**, 2107–2126 (2016).

25. Barrett, E. C. & Lamb, H. H. Climate, history and the modern world. *Geogr. J* **149**, 367 (1983).
26. Brian, E. & Ladurie, E. L. R. Histoire des populations et histoire des savoirs demographiquesHistoire humaine et comparee du climat, Canicules et glaciers XIIIe-XVIIIe siecles. Popul. (French Ed. 60, 837 (2005).
27. Fagan B. The little ice age. How climate made history, 1300–1850. (Basic Books, 2002).
28. Glaser, R. Klimageschichte Mitteleuropas: 1200 Jahre Wetter, Klima, Katastrophen. (WBG, Wissenschaftliche Buchgesellschaft, 2013).
29. Büntgen, U. et al. 2500 years of European climate variability and human susceptibility. *Science (80-.)* **331**, 578–582 (2011).
30. Mörner, N.-A. Solar Minima, earth's rotation and little ice ages in the past and in the future: The North Atlantic–European case. *Glob. Planet. Change* **72**, 282–293 (2010).
31. Schmelzer, N. & Holfort, J. Ice winter severity in the western Baltic Sea in the period of 1301–1500: comparison with other relevant data. *Int. J. Climatol.* **31**, 1094–1098 (2011).
32. Glaser, R. & Kahle, M. Reconstructions of droughts in Germany since 1500-combining hermeneutic information and instrumental records in historical and modern perspectives. *Clim. Past* **16**, 1207–1222 (2020).
33. Steiger, N. J., Smerdon, J. E., Cook, E. R. & Cook, B. I. A reconstruction of global hydroclimate and dynamical variables over the Common Era. *Sci. Data* **5**, 180086 (2018).
34. Hakim, G. J. et al. The last millennium climate reanalysis project: framework and first results. *J. Geophys. Res. Atmos.* **121**, 6745–6764 (2016).
35. Cubasch, U. & Voss, R. The influence of total solar irradiance on climate. *Space Sci. Rev.* **94**, 185–198 (2000).
36. Menary, M. B. & Scaife, A. A. Naturally forced multidecadal variability of the Atlantic meridional overturning circulation. *Clim. Dyn.* **42**, 1347–1362 (2014).
37. Rahmstorf, S. et al. Exceptional twentieth-century slowdown in Atlantic Ocean overturning circulation. (2015). https://doi.org/10.1038/NCLIMATE2554
38. Dima, M. & Lohmann, G. A hemispheric mechanism for the atlantic multidecadal oscillation. *J. Clim.* **20**, 2706–2719 (2007).
39. Vellinga, M. & Wood, R. A. Global climatic impacts of a collapse of the atlantic thermohaline circulation. *Clim. Change* **54**, 251–267 (2002).
40. Moffa-Sánchez, P., Born, A., Hall, I. R., Thornalley, D. J. R. & Barker, S. Solar forcing of North Atlantic surface temperature and salinity over the past millennium. *Nat. Geosci.* **7**, 275–278 (2014).
41. Jackson, L. C. et al. Global and European climate impacts of a slowdown of the AMOC in a high resolution GCM. *Clim. Dyn.* **45**, 3299–3316 (2015).
42. Ionita, M., Lohmann, G., Rimbu, N., Chelcea, S. & Dima, M. Interannual to decadal summer drought variability over Europe and its relationship to global sea surface temperature. *Clim. Dyn.* **38**, 363–377 (2012).
43. Ionita, M., Boroneanț, C. & Chelcea, S. Seasonal modes of dryness and wetness variability over Europe and their connections with large scale atmospheric circulation and global sea surface temperature. *Clim. Dyn.* **45**, 2803–2829 (2015).
44. Kingston, D. G., Stagge, J. H., Tallaksen, L. M. & Hannah, D. M. European-scale drought: understanding connections between atmospheric circulation and meteorological drought indices. *J. Clim.* **28**, 505–516 (2015).
45. Ionita, M., Scholz, P., Lohmann, G., Dima, M. & Prange, M. Linkages between atmospheric blocking, sea ice export through fram strait and the atlantic meridional overturning circulation. *Sci. Rep.* **6**, 32881 (2016).
46. Samaniego, L. et al. Anthropogenic warming exacerbates European soil moisture droughts. *Nat. Clim. Chang* **8**, 421–426 (2018).
47. Neukom, R. et al. Consistent multidecadal variability in global temperature reconstructions and simulations over the Common Era. *Nat. Geosci.* **12**, 643–649 (2019).
48. Gray, S. T., Graumlich, L. J., Betancourt, J. L. & Pederson, G. T. A tree-ring based reconstruction of the Atlantic Multidecadal Oscillation since 1567 A.D. *Geophys. Res. Lett.* **31**, 2–5 (2004).
49. Cook, B. I. et al. Twenty-first century drought projections in the CMIP6 forcing scenarios. Earth's Futur. (2020). https://doi.org/10.1029/2019ef001461
50. Harris, I., Osborn, T. J., Jones, P. & Lister, D. Version 4 of the CRU TS monthly high-resolution gridded multivariate climate dataset. *Sci. Data* **7**, 1–18 (2020).
51. Rayner, N. A. et al. Global analyses of sea surface temperature, sea ice, and night marine air temperature since the late nineteenth century. *J. Geophys. Res.* **108**, 4407 (2003).
52. Slivinski, L. C. et al. Towards a more reliable historical reanalysis: Improvements for version 3 of the Twentieth Century Reanalysis system. *Q. J. R. Meteorol. Soc.* **145**, 2876–2908 (2019).
53. Luterbacher, J. et al. Reconstruction of sea level pressure fields over the Eastern North Atlantic and Europe back to 1500. *Clim. Dyn.* **18**, 545–562 (2002).
54. Casty, C., Wanner, H., Luterbacher, J., Esper, J. & Böhm, R. Temperature and precipitation variability in the European Alps since 1500. *Int. J. Climatol.* **25**, 1855–1880 (2005).
55. Pauling, A., Luterbacher, J., Casty, C. & Wanner, H. Five hundred years of gridded high-resolution precipitation reconstructions over Europe and the connection to large-scale circulation. *Clim. Dyn.* **26**, 387–405 (2006).
56. Glaser, R. & Riemann, D. A thousand-year record of temperature variations for Germany and Central Europe based on documentary data. *J. Quat. Sci.* **24**, 437–449 (2009).
57. Otto-Bliesner, B. L. et al. Climate variability and change since 850 CE: an ensemble approach with the community earth system model. *Bull. Am. Meteorol. Soc.* **97**, 735–754 (2015).
58. Steiger, N. J. et al. Oceanic and radiative forcing of medieval megadroughts in the American Southwest. *Sci. Adv.* **5**, eaax0087 (2019).
59. Tardif, R. et al. Last millennium reanalysis with an expanded proxy database and seasonal proxy modeling. *Clim. Past* **15**, 1251–1273 (2019).
60. Emile-Geay, J. et al. A global multiproxy database for temperature reconstructions of the Common Era. *Sci. Data* **4**, 170088 (2017).
61. Anderson, D. M. et al. Additions to the last millennium reanalysis multi-proxy database. *Data Sci. J* **18**, 1–11 (2019).
62. Landrum, L. et al. Last millennium climate and its variability in CCSM4. *J. Clim.* **26**, 1085–1111 (2012).
63. Lean, J. L. Estimating solar irradiance since 850 CE. *Earth Sp. Sci.* **5**, 133–149 (2018).
64. Crowley, T. J. Causes of climate change over the past 1000 years. *Science (80-.)* **289**, 270–277 (2000).
65. Moffa-Sánchez, P., Hall, I. R., Barker, S., Thornalley, D. J. R. & Yashayaev, I. Surface changes in the eastern Labrador Sea around the onset of the little ice age. *Paleoceanography* **29**, 160–175 (2014).
66. Mann, M. E. et al. Global signatures and dynamical origins of the little ice age and medieval climate anomaly. *Science (80-.)* **326**, 1256 LP–1260 (2009).

Acknowledgements

M.I. and G.L. are supported by Helmholtz funding through the joint program "Changing Earth—Sustaining our Future" (PoF IV) program of the AWI. Funding by the AWI Strategy Fund Project - PalEX and by the Helmholtz Climate Initiative—REKLIM is gratefully acknowledged. V.N. was funded by the project number PN-III-P1-1.1-PD-2019-0469. P.S. has been funded by the Collaborative Research Center TRR 181 "Energy Transfer in Atmosphere and Ocean".

Author contributions

M.I. designed the study and wrote the paper. P.S. wrote the code for the data analysis. M.D., V.N., P.S., and G.L. helped write the paper and interpret the results.

Funding

Open Access funding enabled and organized by Projekt DEAL.

Competing interests

The authors declare no competing interests.

Additional information

Supplementary information The online version contains supplementary material available at https://doi.org/10.1038/s43247-021-00130-w.

Correspondence and requests for materials should be addressed to M.I.

Peer review information Primary handling editor: Heike Langenberg.

Reprints and permission information is available at http://www.nature.com/reprints

Publisher's note Springer Nature remains neutral with regard to jurisdictional claims in published maps and institutional affiliations.

Open Access This article is licensed under a Creative Commons Attribution 4.0 International License, which permits use, sharing, adaptation, distribution and reproduction in any medium or format, as long as you give appropriate credit to the original author(s) and the source, provide a link to the Creative Commons license, and indicate if changes were made. The images or other third party material in this article are included in the article's Creative Commons license, unless indicated otherwise in a credit line to the material. If material is not included in the article's Creative Commons license and your intended use is not permitted by statutory regulation or exceeds the permitted use, you will need to obtain permission directly from the copyright holder. To view a copy of this license, visit http://creativecommons.org/licenses/by/4.0/.

© The Author(s) 2021

Supplementary file

Past megadroughts in central Europe were longer, more severe and less warm than modern droughts

M. Ionita[1*], M. Dima[1,2], V. Nagavciuc[1,3], P.Scholz[1] and G. Lohmann[1,4]

[1] Alfred Wegner Institute Helmholtz Center for Polar and Marine Research, Bremerhaven, Germany
[2] Faculty of Physics, Bucharest University, Bucharest, Romania
[3] Faculty of Forestry, Ștefan cel Mare University, Universității Str. 13, 720229, Suceava, Romania
[4] MARUM, Bremen University, Bremen, Germany

[*] Corresponding author
E-mail: Monica.Ionita@awi.de

1. Characteristics of the driest years in Europe, over the last millennium

Information regarding the occurrence of extreme droughts and high temperatures for some of the driest years (e.g. 1503, 1517, 1865, 1921) can be inferred from observational data, documentary sources and climate reconstructions for the last millennium. According to an "ancient book of memory", the summer 1503 was so dry that "people could not remember such a dry summer for 30 years, there was bad harvest and the wine was very good that year"[1]. The winter 1503 was extremely cold and the summer was very dry and warm over the central part of Europe, due to a high pressure system center over the central part of Europe[2]. Year 1517 was characterized by a cold winter, followed by an extremely dry and warm April and ground freezing in May. The beginning of the summer was dry and warm with dramatic consequences for the society (bad harvest and lack of pastures)[2]. The winter 1864/65 was very long lasting until the end of March. Afterwards the weather became exceptionally warm and dry. The number of summer days was accordingly high (e.g. 103 days in Stuttgart)[3]. At Zürich meteorological station, between January 1864 and July 1865, all months have been characterized by below normal precipitation. Glaser et al.(2017)[3] have shown that the heat and the harvest failure of 1865 led to a migration peak in the south-western part of Germany, due to an increase in the prices in the following years. 1921 is considered as a year of unprecedented small rainfall over the south-east of England[4]. The whole of Wales, most of England and large areas in the East Midlands, of Scotland and Ireland had less than a quarter of their average precipitation, while considerable areas in the north and the south-west of England and Wales received less than 10% of normal precipitation. Casty et al. (2005)[5] concluded that the years 1540, 1921 and 2003 were very likely to have been the driest in the context of the past 500 years in the Greater Alpine area. Year 1921 is also the driest one over the last 200 years, in terms of low flow situations, over the Rhine and Weser rivers catchment area (Supplementary Figure 3).

2. The robustness of composite the composite maps relative to the phases of TSI extremes in solar reconstructions

The composite maps of Z500 shown in Figure 6 represents a key link between solar variability and climate. The close similarity between the Z500 center of positive values derived based on the reconstructed PDSI index[6] (Figure 6a) with that obtained using the reconstructed TSI[7] (Figure 6b), is consistent with the physical mechanism relating this Z500 high with central Europe drought conditions. Furthermore, the same structure appears to manifest not only during winter, but also for spring and summer (Supplementary Figure 8). The mechanism emerging from our study, based on analyzes of instrumental, reconstructed and proxy data, involves a response of AMOC to TSI changes and then an atmospheric baroclinic response to cold North Atlantic Ocean conditions manifested as a center of high pressure/Z500 located over eastern North Atlantic and western Europe. Elements of this mechanism, and specifically this atmospheric structure, are reproduced by numerical experiments[8] investigating the climate response at millennial time scales to changes of the solar forcing, without any dependence on potential uncertainties regarding the timing of TSI maxima and minima. As part of this mechanism, the same atmospheric structure is derived in response to cold ocean conditions associated with a reduced AMOC state in numerical simulations[9]. Therefore, these model integrations indicate that the structure and localization of the atmospheric center of high Z500 is not affected by potential varying timings of solar maxima/minima in different solar reconstructions.

The composite maps shown in Figure 6 support the role played by the center of Z500 anomalies in generating drought conditions in central Europe: positive Z500 anomalies imply reduced upward motions in the atmosphere and therefore reduced precipitations. One notes that, as atmospheric processes, these are manifesting rapidly (days-to-weeks), regardless of the time scale of the forcing which excites them. This implies that although the composite maps (Figure 6) are constructed based on data which includes year-to-year variability, they are representative also for longer time scales. This is supported by the fact that model simulations emphasize the atmospheric center of positive values also in association with decadal-to-millennial variability[8–10].

3. North Atlantic SSTs and the megadroughts

The two megadroughts over the central part of Europe and their relationship with the prevailing SSTs in the North Atlantic basin are visible also in two paleo reanalyzes of the last millennium (Supplementary Figure 7 and Supplementary Figure 9)[11,12], although the amplitude of the megadroughts in the paleo reanalysis data is smaller compared to the amplitude of these two events in the Old World Drought Atlas (OWDA) reconstruction (Supplementary Figure 7). The prevailing SSTs, in the PHYDA paleo reanalysis, during the two megadrought events are characterized by widespread cold anomalies in the North Atlantic basin, although warmer SSTs are observed around Fennoscandia and in the Gulf Stream region (Supplementary Figure 9). The warm SSTs in the Gulf Stream regions are likely caused by atmospheric conditions linked to NAO, which is influenced by changes in the solar forcing [13]. Furthermore, the timing of the ocean and continental climate variability suggests that the ocean conditions, characterized by a declining AMOC state (Figure 5d), and a cold North Atlantic basin (Figure 5e and 5f, Supplementary Figure 9), were among the driving factors responsible for modulating the climate

over the central and western part of Europe on decadal to multidecadal time scales. Over the period 1000 – 2000, dry summers (PDSI < 25th percentile) over the analyzed region occur in association with a negative phase of AMO and reduced solar irradiance, while wet summers (PDSI > 75th percentile) occur in association with a positive phase of AMO and increased solar irradiance (Supplementary Figure 10). The box plot and the Gaussian distribution shows that there is a significant difference ($p \ll 0.001$, based on a two samples Kolmogorov and Smirnov test) in the distribution of the winter AMO index and TSI for the two extreme cases (dry vs. wet years).

4. Present-day conditions

To identify the coupled patterns of variability of the summer drought, the previous winter SST and the large-scale atmospheric circulation, over the observational record, we used a Canonical Correlation Analysis (CCA). CCA is a powerful multivariate technique used to identify pairs of patterns with the maximum correlation between their associated time series[14]. As the core constraints of the method are the maximization of the correlation, the corresponding patterns are provided by the method even if they do not explain the main part of the variance in their fields. Patterns with a large percentage of variance explained don't necessarily appear in the first pairs. In our study, we used CCA to identify coupled pairs of modes of variability, for the observational record (Supplementary Figure 11). Before applying a CCA, the dimensionality of the observed scPDSI, sea surface temperature (SST), precipitation (PP), and geopotential height at 500mb (Z500) datasets were reduced by an Empirical Orthogonal Function (EOF) analysis. The first 15 EOFs of the summer scPDSI and winter SST, winter PP and winter Z500 are retained as an input into the CCA, for the observation period. The first 15 EOFs capture approximately 80% of the total variance for summer scPDSI and more than 70% of the winter SST, winter PP, and winter Z500 variability. The optimum number of retained EOFs was chosen so that using one more EOF would not change significantly the canonical correlation[15]. Among other statistical methods, CCA has the advantage to select pairs of optimally correlated spatial patterns, which may lead to a physical interpretation of the mechanism controlling the climate variability.

On multidecadal time scales, AMO/AMOC plays a significant role in the occurrence of dry and wet periods, especially over the central part of Europe. Based on the CCA analysis, we show that dry (wet) summers (Supplementary Figure 11a) are associated with a cold (warm) North Atlantic basin in the previous winter (Supplementary Figure 11b), reduced (enhanced) winter precipitation over the central part of Europe (Supplementary Figure 11c) and enhanced blocking over the central and northern part of Europe (Supplementary Figure 11d). The link between cold North Atlantic conditions and European scale drought are supported also by previous studies based on observational data[16–18]. In previous studies, it was shown that during the negative phase of AMO (cold North Atlantic basin) Germany and the southern part of the Scandinavian Peninsula is affected by dryness, while a warm North Atlantic basin (positive AMO phase) is associated with wetness over these regions[19].

a)

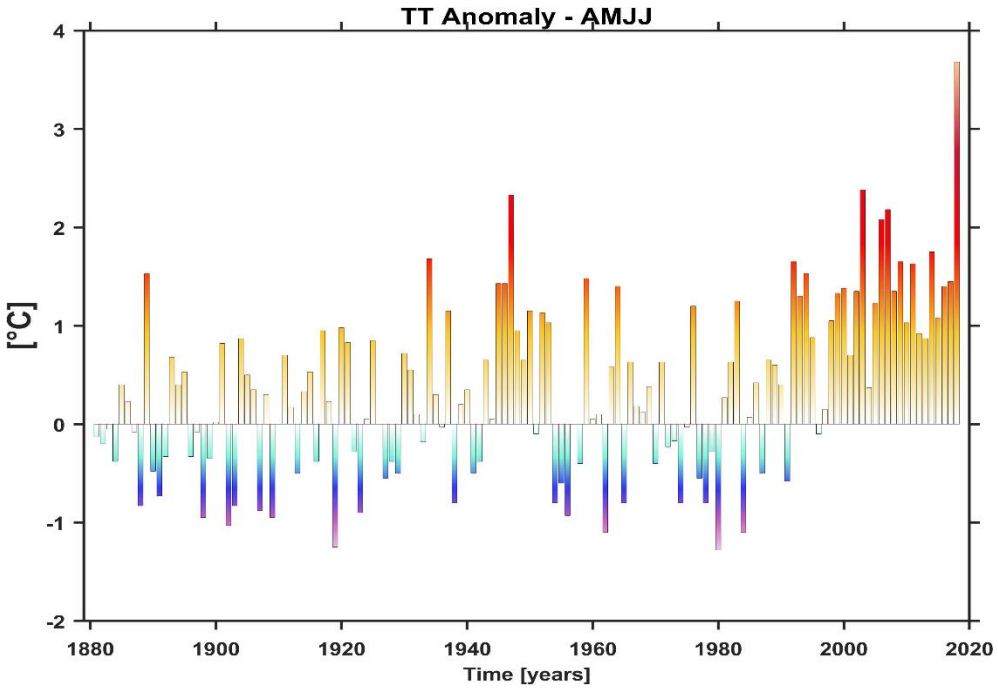

b)

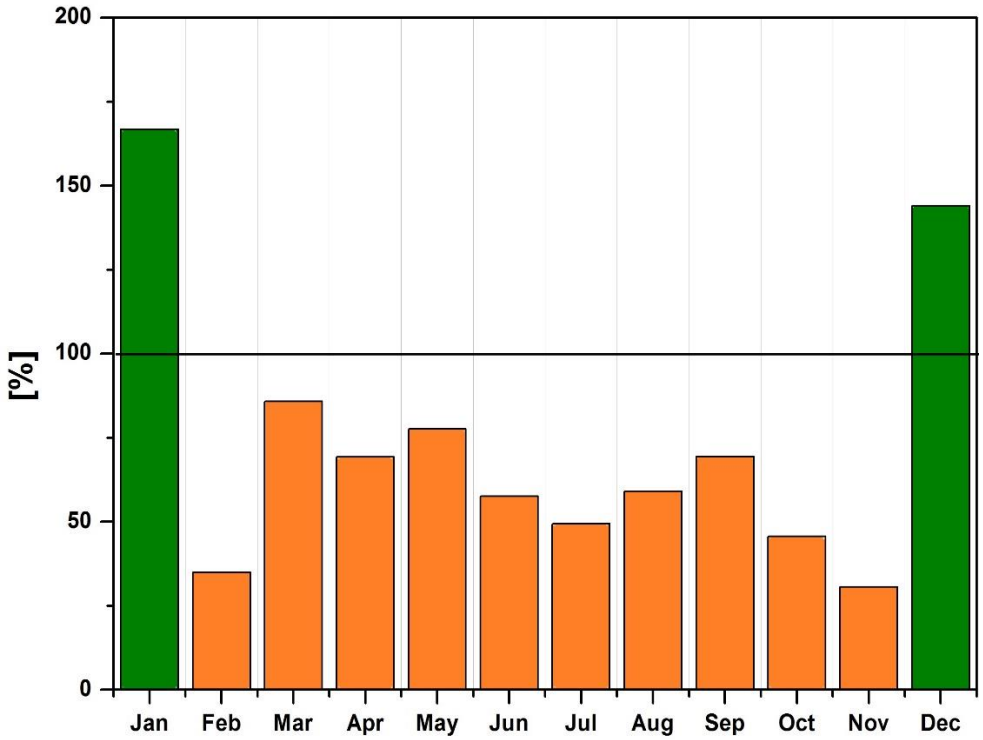

Supplementary Figure 1. Regional climate variability. a) Air temperature anomaly, for Germany, averaged over the months April-May-June-July (AMJJ) over the 1880 – 2018 period. AMJJ 2018 ranks as the hottest year on record and b) Percentage of the monthly precipitation for the year 2018 for Germany, relative to the climatology over the 1971 – 2000 period.
Data source: https://opendata.dwd.de/climate_environment/CDC/.

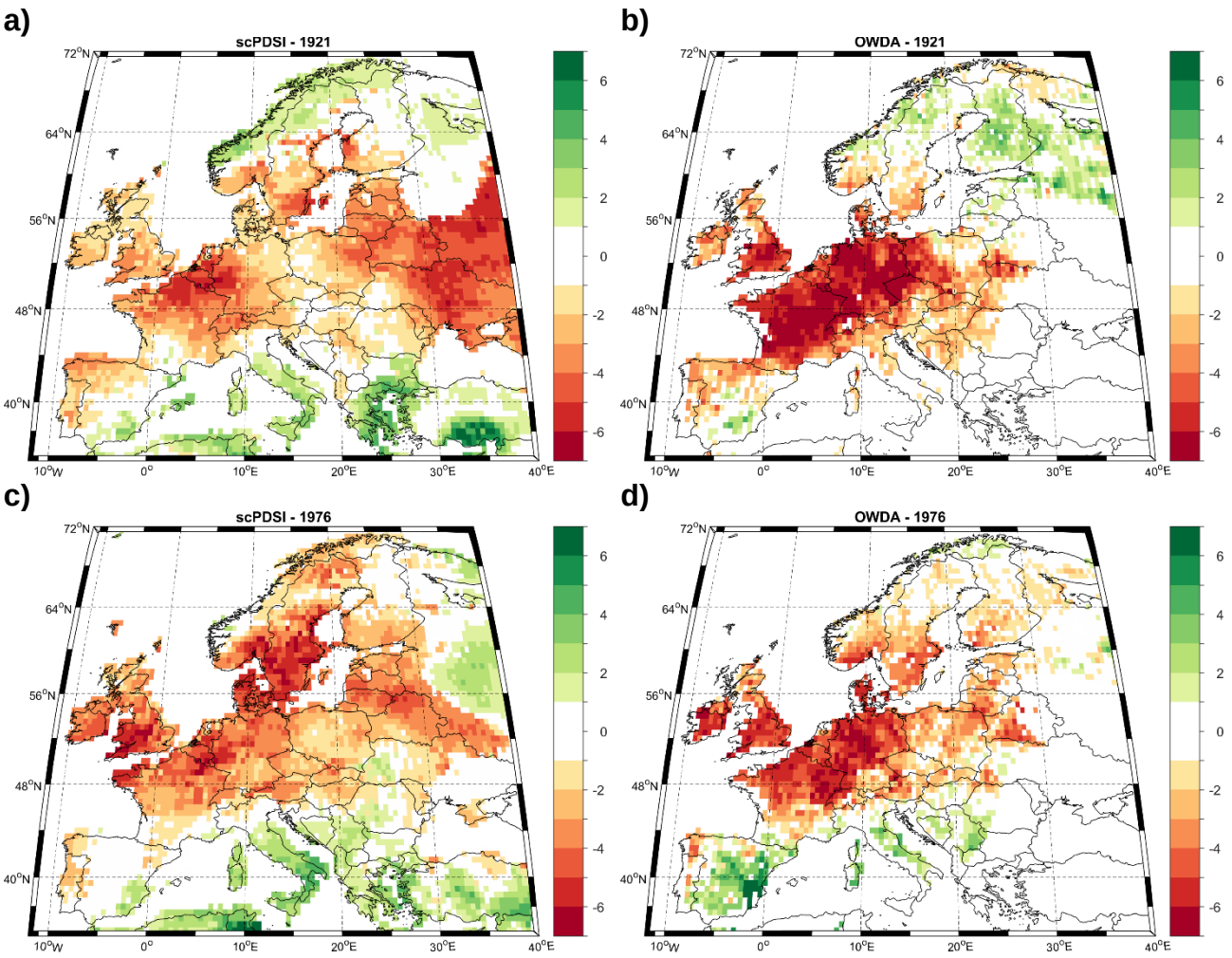

Supplementary Figure 2. Dry events in the 20th century. The self-calibrated Palmer Drought Severity Index (scPDSI) for summer 1921 for a) observational data[20] and b) the Palmer Drought Severity Index based on the Old World Drought Atlas (OWDA)[6]; c) and d) same as in a) and b) for summer 1976.

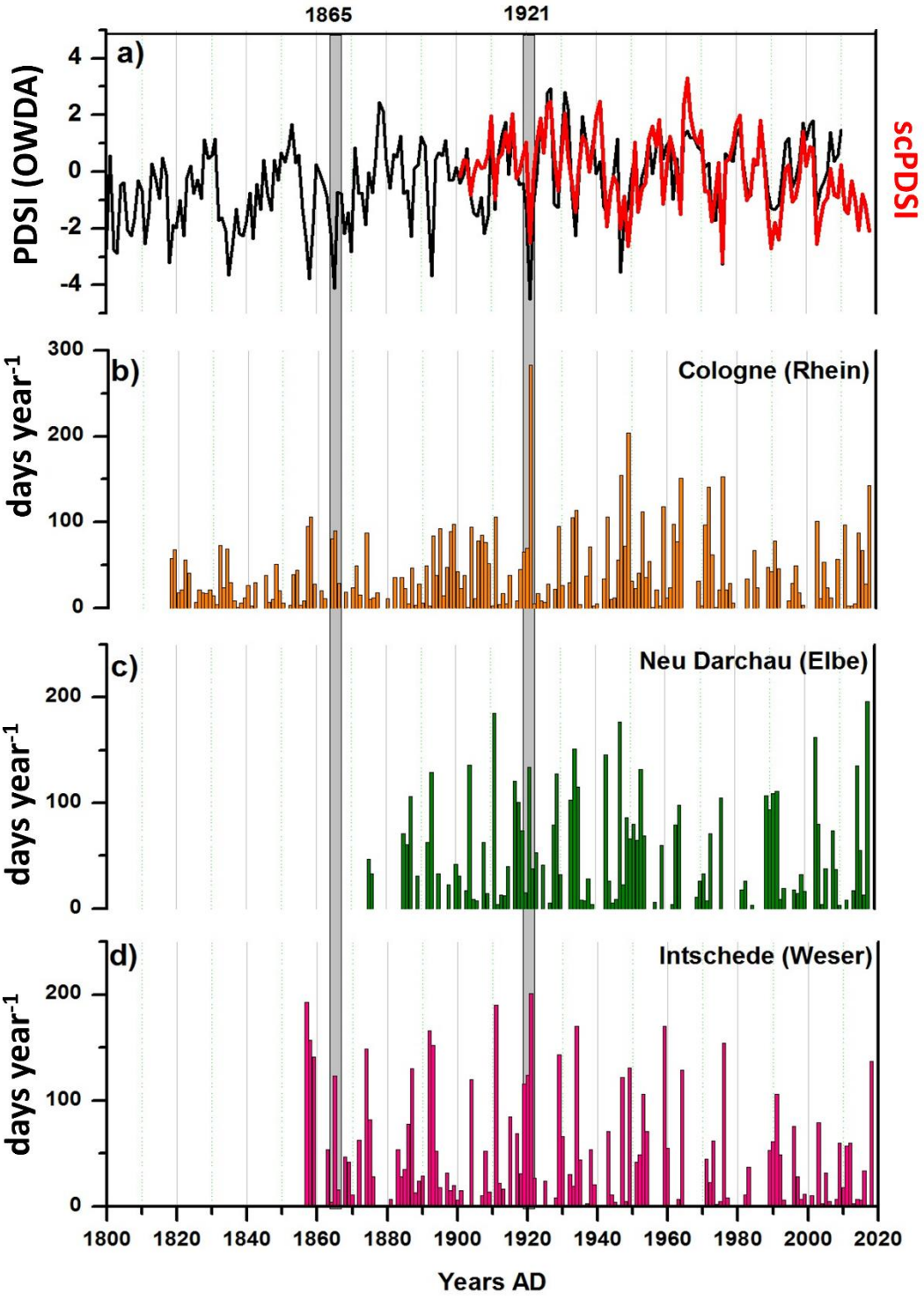

Supplementary Figure 3. Streamflow variability. a) Regional mean Old World Drought Atlas (OWDA) drought index for central Europe (3°E - 20°E, 45°N - 56°N, black line) for the 1800 – 2012 period and the instrumental June through August scPDSI (solid red line) for the 1901 - 2018 period; Number of days /year when the daily streamflow < Q70 (the 30 percentile streamflow) for b) Cologne (Rhine); c) Neu Darchau (Elbe) and d) Intschede (Weser).
Data source: https://www.bafg.de/GRDC/EN/Home/homepage_node.html).

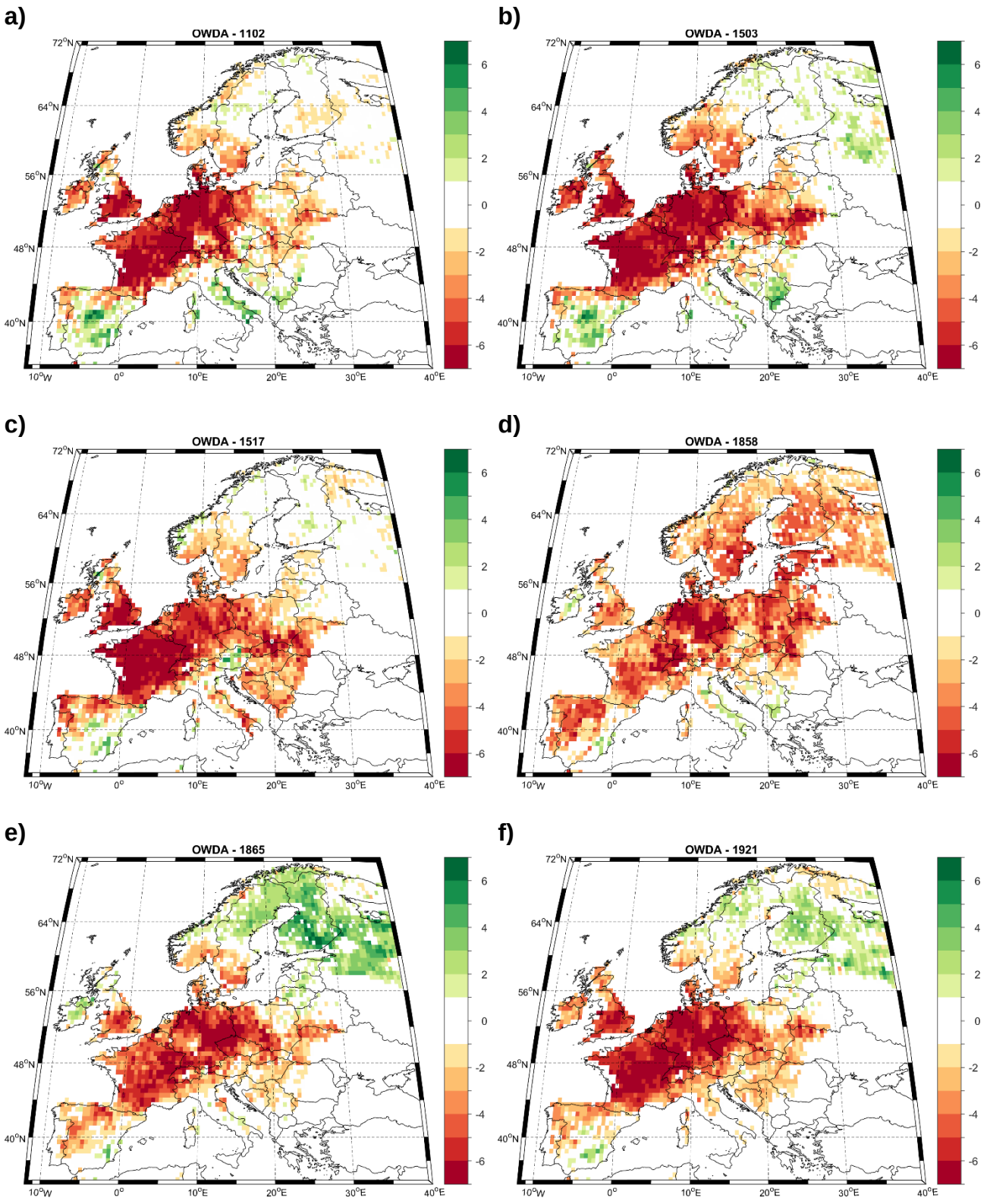

Supplementary Figure 4. Extreme dry events. The spatial extent of the drought conditions at European level for the 6 driest years based on the reconstructed PDSI data (OWDA)[6]: 1102, 1503, 1517, 1858, 1865 and 1921.

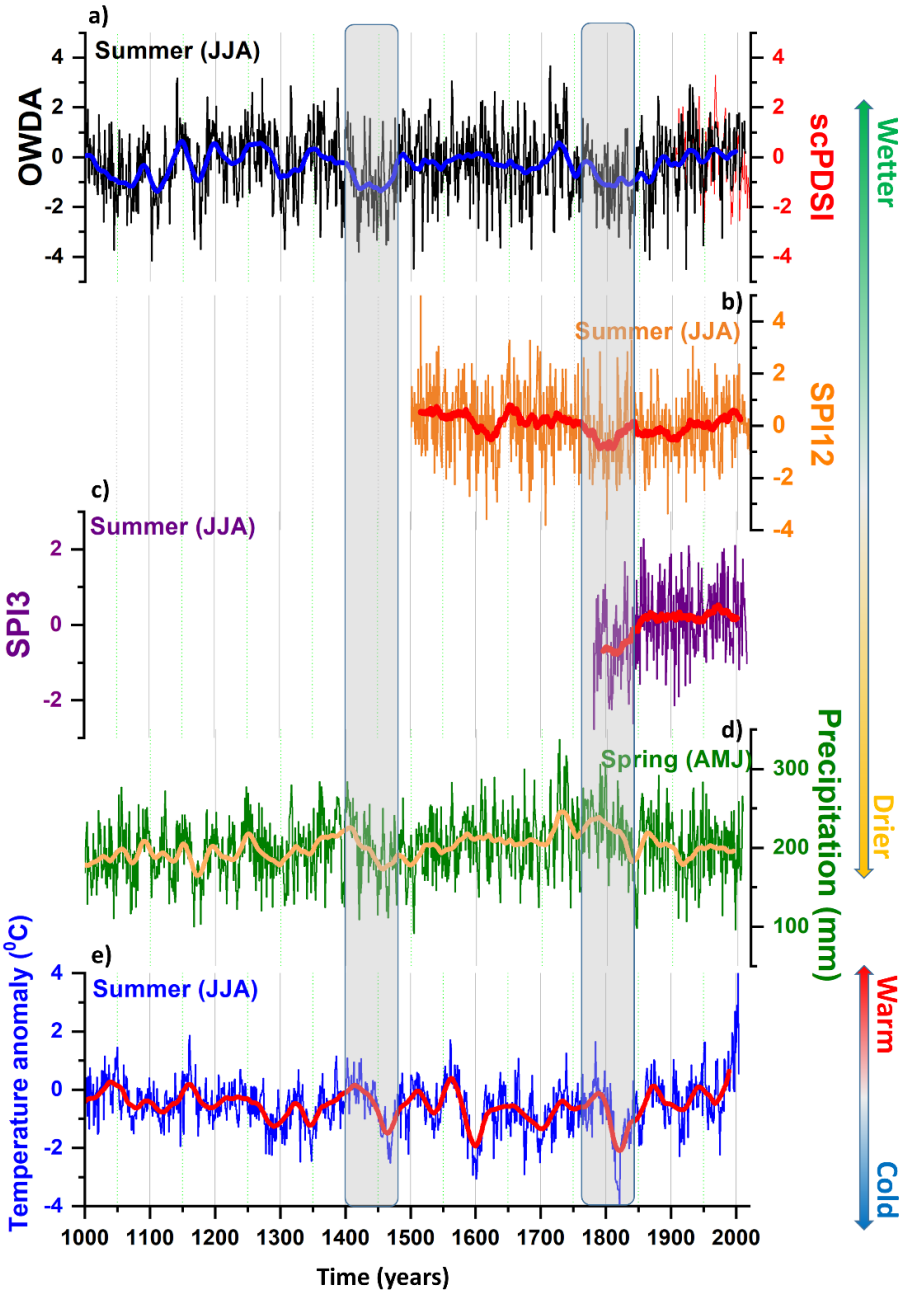

Supplementary Figure 5. Climate variability over the last millennium. a) Regional mean PDSI index based on the Old World Drought Atlas (OWDA)[6] for central Europe (3°E - 20°E, 45°N - 56°N, black line) for the 1000 - 2012 period and the instrumental June through August[20] scPDSI (solid red line) for the 1901 - 2018 period; b) The reconstructed summer Standardized Precipitation Index over Germany for the 1500 – 2019 period[21]; c) The reconstructed summer Standardized Precipitation Index at Żagań/Wrocław (Poland) for the 1781 – 2015 period[22]; d) Reconstructed April – May - June precipitation totals and e) June – July - August temperature anomalies with respect to the 1901 – 2000 period, over the central part of Europe. The time series in b) is obtained by combining different records (tree-ring proxy and instrumental records) averaged over the region 8°E - 10°E and 45° - 50°N. Bold lines in a), b), c), d) and f) represent the 31-year running mean. The seasonal spring precipitation and summer temperature anomalies in d) and e) are based on the reconstruction of Büntgen et al. (2011)[23].

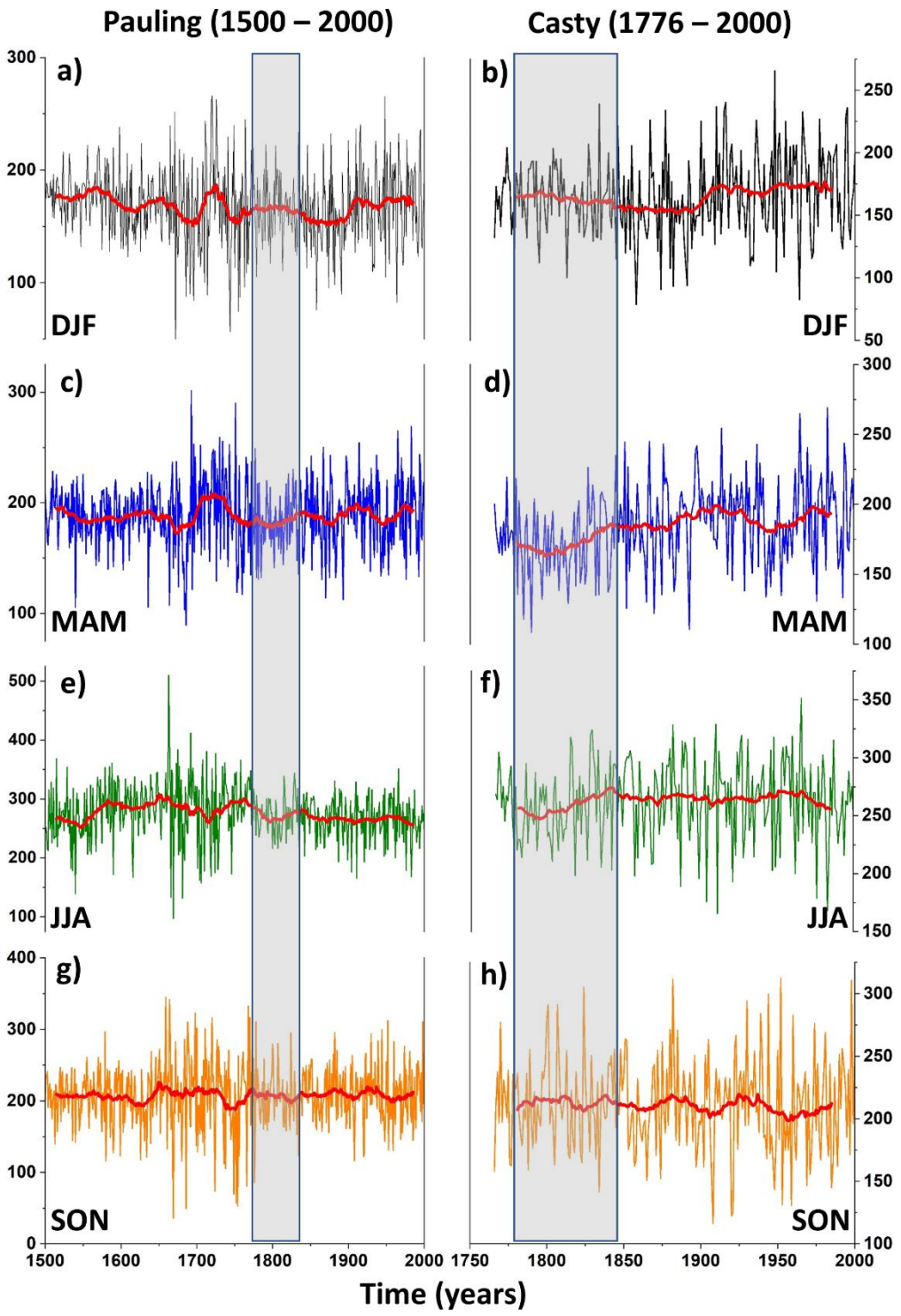

Supplementary Figure 6. Precipitation variability over the last 500 years. Time series of seasonal precipitation, averaged over central Europe (3°E - 20°E, 45°N - 56°N), based on two paleo reconstructions: left column (Pauling et al., 2006)[24] and right column (Casty et al., 2005)[5]. The red bold line represents the 31 years running mean. Units: mm season^{-1}.

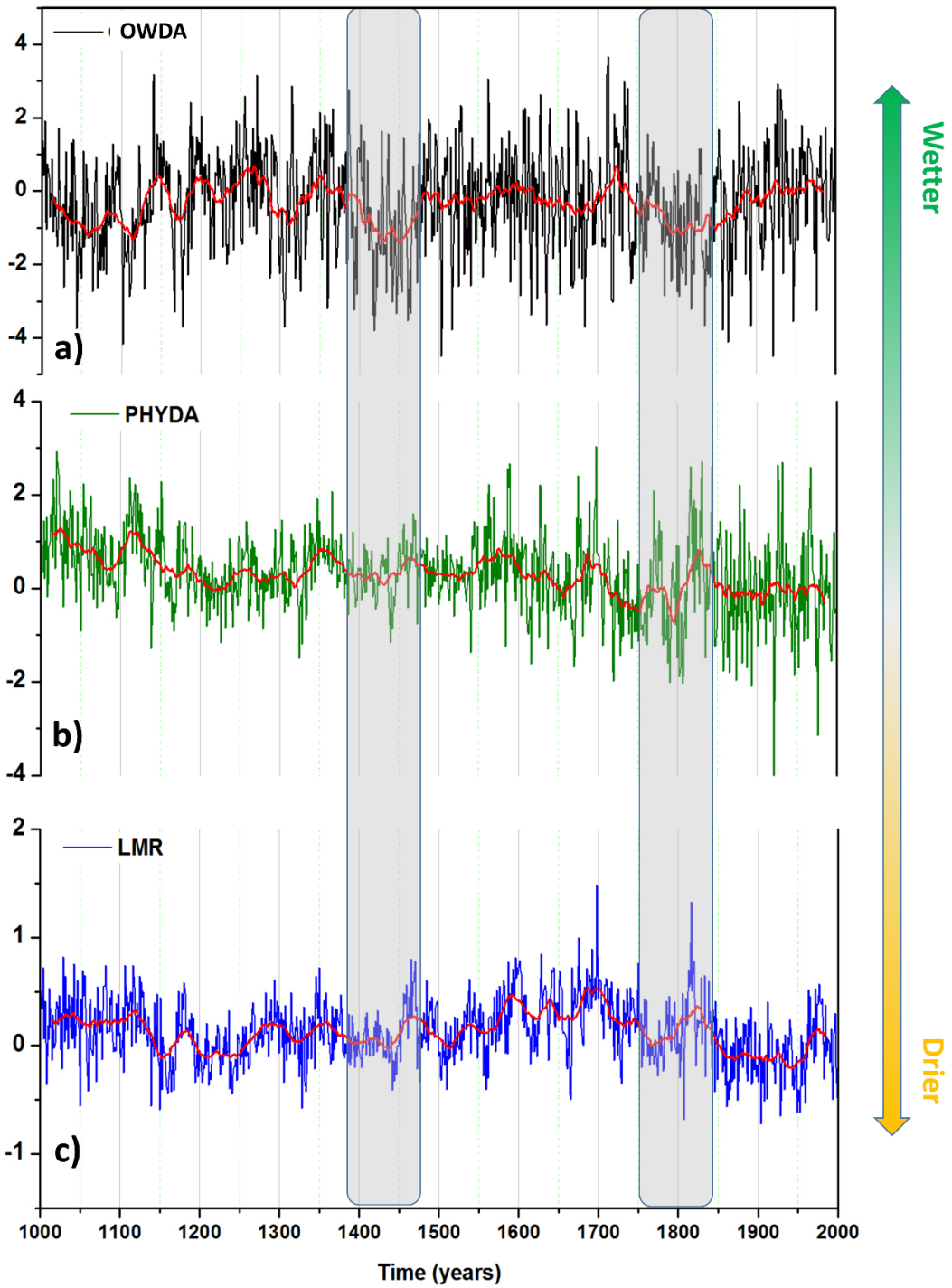

Supplementary Figure 7. Drought variability over the last millennium. a) Regional mean Old World Drought Atlas (OWDA)[6] summer PDSI for central Europe (3°E - 20°E, 45°N - 56°N); b) as in a) but for the summer (JJA) PDSI extracted from the PHYDA paleo reanalysis[11] and c) as in a) but for the annual PDSI extracted from the LMR paleo reanalysis data[12]. The red line in a), b) and c) represents the 31 years running mean of each time series.

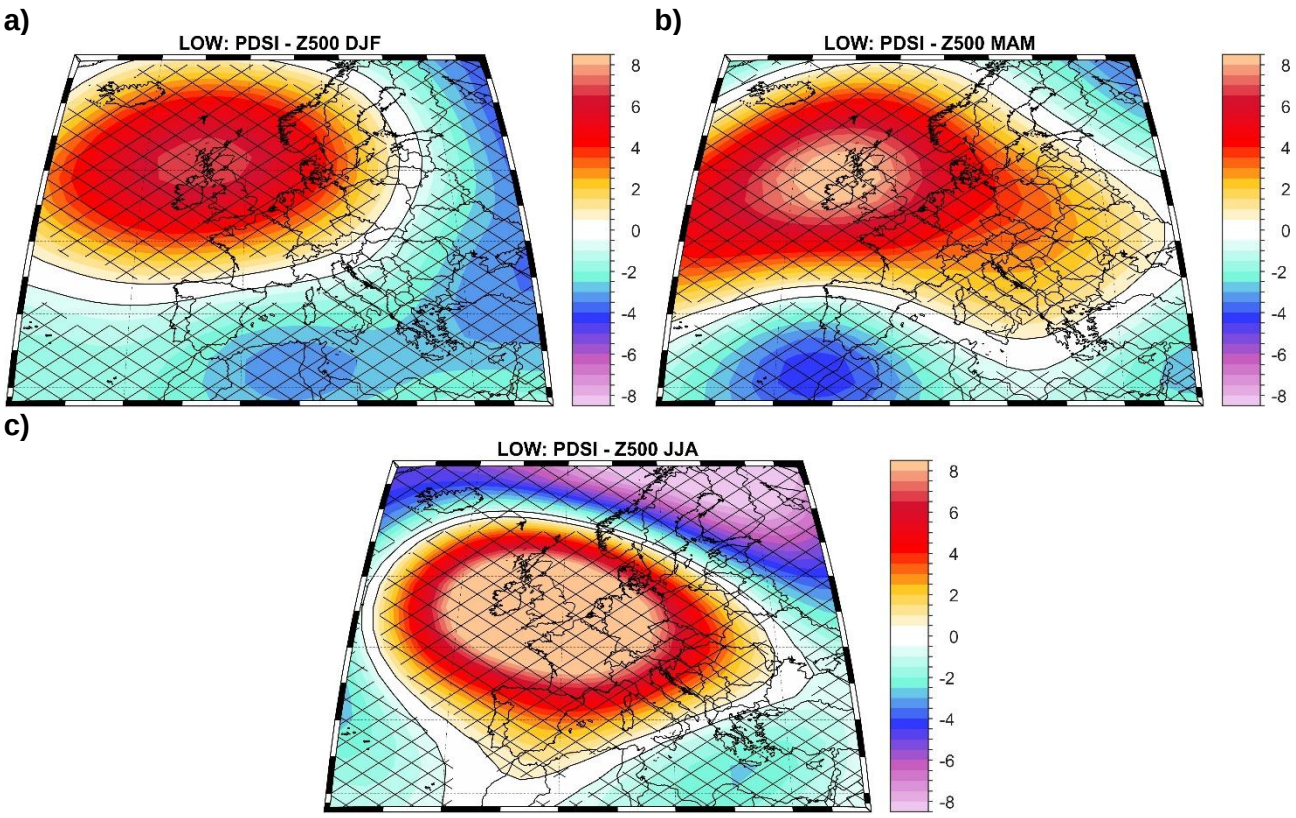

Supplementary Figure 8. **Large-scale climate drivers of dry events.** a) The composite map between the reconstructed[6] low PDSI index (PDSI < − 0.75 std. dev.) and winter (DJF) reconstructed Geopotential Height at 500mb (Z500)[25]; b) as in a) but for spring (MAM) reconstructed Geopotential Height at 500mb (Z500) and c) as in a) but for summer (JJA) reconstructed Geopotential Height at 500mb (Z500). Units: Z500 (m).

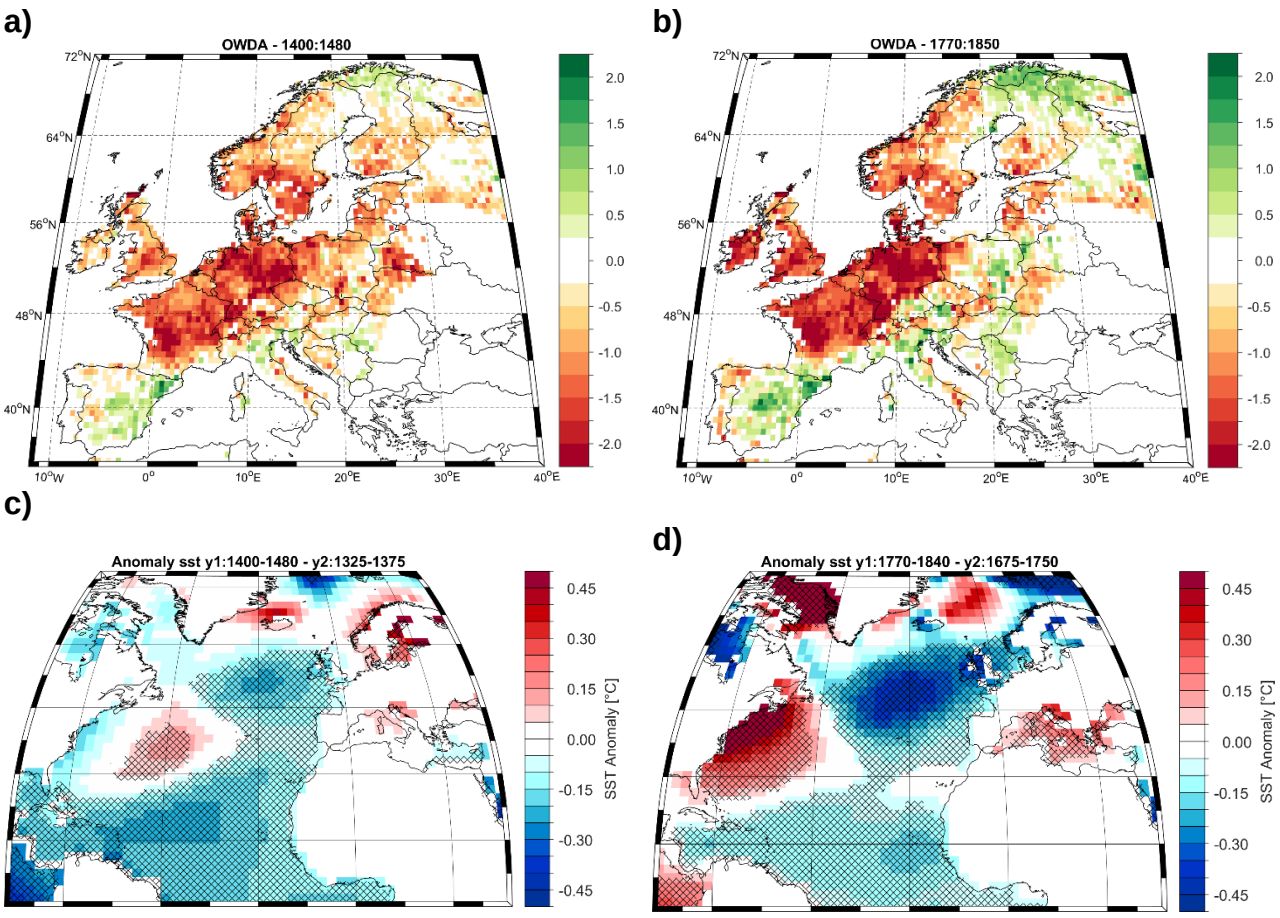

Supplementary Figure 9. Megadroughts and oceanic drivers. a) Average summer (JJA) PDSI over the 1400 – 1500 period, based on the ODWA data[6]; b) as in a) but for the 1770 – 1850 period; c) Winter (DJF) SST anomaly over the 1400 – 1500 period based on the PHYDA data set[11] and d) as in c) but for the 1770 – 1850 period. The SST anomalies in c) are computed relative to the 1325 – 1375 period and the SST anomalies in d) are computed relative to the 1675 – 1750 period. The hatching highlights significant values at a confidence level of 95 %.

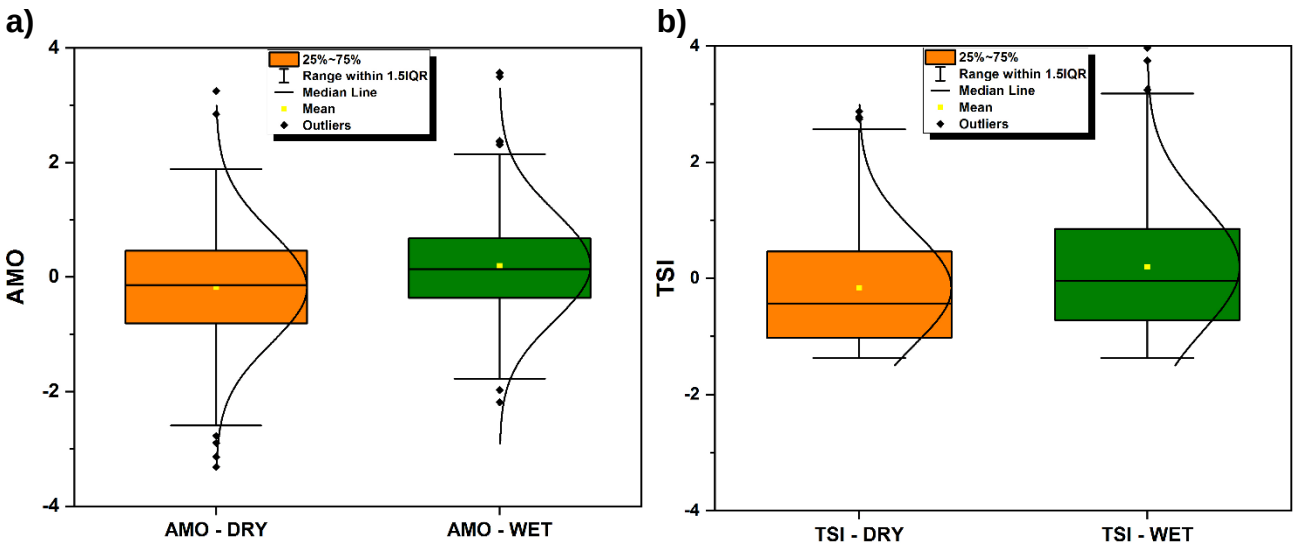

Supplementary Figure 10. Dry years and the Atlantic Multidecadal Oscillation. a) Box plot and Gaussian situation of the Atlantic Multidecadal Oscillation (AMO) based on the PHYDA paleo reanalysis data[11] for the years when PDSI index < 25th percentile (AMO – DRY, orange) and for the years when PDSI index > 75th percentile (AMO – WET, green) and b) same as in a) but for the reconstructed TSI[7]. The box plot and the Gaussian distribution indicates that there is a significant difference ($p \ll 0.001$, Kolmogorov-Smirnov) in the distribution of the winter AMO index[11] and TSI[7] for the two extreme cases (dry vs. wet years).

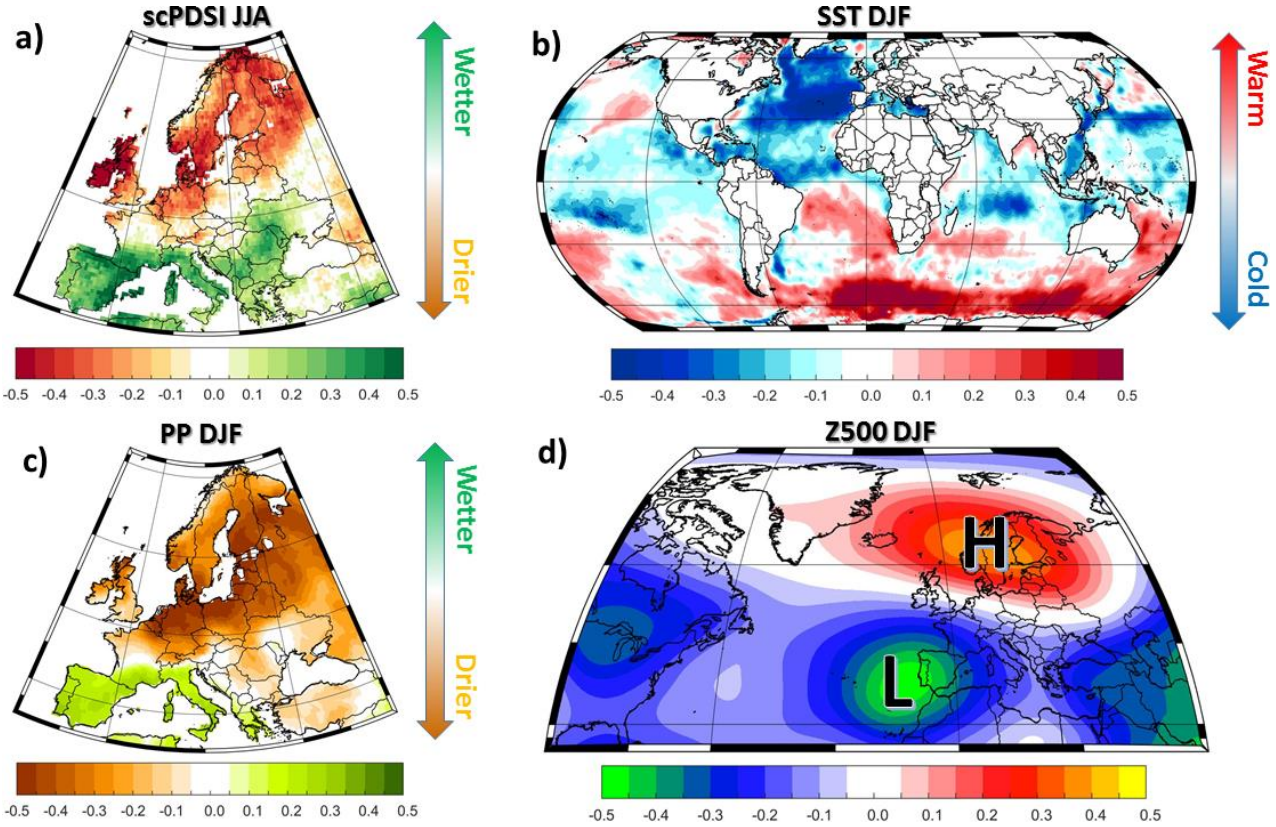

Supplementary Figure 11. Couple modes of variability. The first coupled mode of variability (CCA) between a) summer scPDSI[20], b) winter SST[26], c) Winter PP[20] and d) Winter Z500[27]. The analysis is performed over the 1901 – 2015 period. Summer scPDSI is treated as a predictor and winter SST, winter PP and Z500 as predictands. The first 15 EOF modes of the summer scPDSI and winter SST, winter PP and winter Z500 are retained as an input into the CCA. The first 15 EOFs capture approximately 80% of the total variance for summer scPDSI and more than 70% of the winter SST, winter PP and winter Z500 variability.

References

1. Brázdil, R., Kiss, A., Luterbacher, J., Nash, D. J. & Řezníčková, L. Documentary data and the study of the past droughts: an overview of the state of the art worldwide. Clim. Past Discuss. 1–67 (2018). doi:10.5194/cp-2018-118

2. Glaser, R. Klimageschichte Mitteleuropas : 1200 Jahre Wetter, Klima, Katastrophen. (WBG, Wissenschaftliche Buchgesellschaft, 2013).

3. Glaser, R., Himmelsbach, I. & Bösmeier, A. Climate of migration? How climate triggered migration from southwest Germany to North America during the 19th century. Clim. Past **13**, 1573–1592 (2017).

4. Brooks, C. E. P. & Glasspoole, J. The drought of 1921 in the British Isles. Mon. Weather Rev. **50**, 93–93 (1922).

5. Casty, C., Wanner, H., Luterbacher, J., Esper, J. & Böhm, R. Temperature and precipitation variability in the European Alps since 1500. Int. J. Climatol. **25**, 1855–1880 (2005).

6. Cook, E. R. et al. Old World megadroughts and pluvials during the Common Era. Sci. Adv. (2015). doi:10.1126/sciadv.1500561

7. Lean, J. L. Estimating Solar Irradiance Since 850 CE. Earth Sp. Sci. **5**, 133–149 (2018).

8. Moffa-Sánchez, P., Hall, I. R., Barker, S., Thornalley, D. J. R. & Yashayaev, I. Surface changes in the eastern Labrador Sea around the onset of the Little Ice Age. Paleoceanography **29**, 160–175 (2014).

9. Jackson, L. C. et al. Global and European climate impacts of a slowdown of the AMOC in a high resolution GCM. Clim. Dyn. **45**, 3299–3316 (2015).

10. Moffa-Sánchez, P., Born, A., Hall, I. R., Thornalley, D. J. R. & Barker, S. Solar forcing of North Atlantic surface temperature and salinity over the past millennium. Nat. Geosci. **7**, 275–278 (2014).

11. Steiger, N. J., Smerdon, J. E., Cook, E. R. & Cook, B. I. A reconstruction of global hydroclimate and dynamical variables over the Common Era. Sci. Data **5**, 180086 (2018).

12. Hakim, G. J. et al. The last millennium climate reanalysis project: Framework and first results. J. Geophys. Res. Atmos. **121**, 6745–6764 (2016).

13. Kodera, K. Solar influence on the spatial structure of the NAO during the winter 1900–1999. Geophys. Res. Lett. **30**, (2003).

14. von Storch, H. & Zwiers, F. W. Statistical Analysis in Climate Research. Statistical Analysis in Climate Research (Cambridge University Press, 1999). doi:10.1017/cbo9780511612336

15. Wilks, D. S. Statistical methods in the atmospheric sciences. (Elsevier Academic Press, 2011).

16. Ionita, M., Lohmann, G., Rimbu, N., Chelcea, S. & Dima, M. Interannual to decadal summer drought variability over Europe and its relationship to global sea surface

temperature. Clim. Dyn. **38**, 363–377 (2012).

17. Ionita, M., Boroneanț, C. & Chelcea, S. Seasonal modes of dryness and wetness variability over Europe and their connections with large scale atmospheric circulation and global sea surface temperature. Clim. Dyn. **45**, 2803–2829 (2015).

18. Kingston, D. G., Stagge, J. H., Tallaksen, L. M. & Hannah, D. M. European-Scale Drought : Understanding Connections between Atmospheric Circulation and Meteorological Drought Indices. J. Clim. **28**, 505–516 (2015).

19. Ionita, M., Scholz, P., Lohmann, G., Dima, M. & Prange, M. Linkages between atmospheric blocking, sea ice export through Fram Strait and the Atlantic Meridional Overturning Circulation. Sci. Rep. **6**, 32881 (2016).

20. Harris, I., Osborn, T. J., Jones, P. & Lister, D. Version 4 of the CRU TS monthly high-resolution gridded multivariate climate dataset. Sci. Data **7**, 1–18 (2020).

21. Glaser, R. & Kahle, M. Reconstructions of droughts in Germany since 1500-combining hermeneutic information and instrumental records in historical and modern perspectives. Clim. Past **16**, 1207–1222 (2020).

22. Przybylak, R. et al. Droughts in the area of Poland in recent centuries in the light of multi-proxy data. Clim. Past **16**, 627–661 (2020).

23. Büntgen, U. et al. 2500 years of European climate variability and human susceptibility. Science (80-.). **331**, 578–582 (2011).

24. Pauling, A., Luterbacher, J., Casty, C. & Wanner, H. Five hundred years of gridded high-resolution precipitation reconstructions over Europe and the connection to large-scale circulation. Clim. Dyn. **26**, 387–405 (2006).

25. Luterbacher, J. et al. Reconstruction of sea level pressure fields over the Eastern North Atlantic and Europe back to 1500. Clim. Dyn. **18**, 545–562 (2002).

26. Rayner, N. A. et al. Global analyses of sea surface temperature, sea ice, and night marine air temperature since the late nineteenth century. J. Geophys. Res. **108**, 4407 (2003).

27. Slivinski, L. C. et al. Towards a more reliable historical reanalysis: Improvements for version 3 of the Twentieth Century Reanalysis system. Q. J. R. Meteorol. Soc. **145**, 2876–2908 (2019).